

# Thermal-Drift Sampling: Generating Random Thermal Ensembles for Quantum Chaos Diagnostics

Jiyu Jiang,<sup>1</sup> Mingrui Jing,<sup>1</sup> Jizhe Lai,<sup>1</sup> Xin Wang,<sup>1,\*</sup> and Lei Zhang<sup>1</sup>

<sup>1</sup>Thrust of Artificial Intelligence, Information Hub,

The Hong Kong University of Science and Technology (Guangzhou), Guangzhou 511453, China

(Dated: February 6, 2026)

Random thermal states of many-body Hamiltonians underpin studies of thermalization, chaos, and quantum phase transitions, yet their generation remains costly when each Hamiltonian must be prepared individually. We introduce the thermal-drift channel, a measurement-based operation that implements a tunable nonunitary drift along a chosen Pauli term. Based on this channel, we present a measurement-controlled sampling algorithm that generates thermal states together with their Hamiltonian “labels” for general physical models. We prove that the total gate count of our algorithm scales cubically with system size, quadratically with inverse temperature, and as the inverse error tolerance to the two-thirds power, with logarithmic dependence on the allowed failure probability. We also show that the induced label distribution approaches a normal distribution reweighted by the thermal partition function, which makes an explicit trade-off between accuracy and effective range. Numerical simulations for a 2D Heisenberg model validate the predicted scaling and distribution. As an application, we compute unfolding-free level-spacing ratio statistics from sampled thermal states of a 2D transverse-field Ising model and observe a crossover toward the Wigner–Dyson prediction, demonstrating a practical and scalable route to chaos diagnostics and random matrix universality studies on near-term quantum hardware.

**Introduction.**— Considerable attention has been directed toward the generation of random quantum states, which offers a resource analogous to random numbers in classical stochastic theories [1]. Ensembles of random pure states underpin our understanding of quantum complexity, chaos [2], and quantum metrology [3], with direct relevance to quantum circuits [4, 5], black-hole physics [6], and quantum supremacy experiments [7, 8]. Haar random states exhibit universal entanglement and spectral properties predicted by random matrix theory, making them indispensable for benchmarking quantum devices [5, 9] and probing the limits of classical simulability [1, 10]. As quantum processors scale up, the controlled generation of such random pure states has become both a theoretical testbed for many-body physics and a practical diagnostic for near-term quantum hardware [4].

While pure states are idealized, random mixed states effectively describe realistic quantum many-body systems, elucidating thermalization and phase structures [11]. Within this domain, random thermal states are essential due to their connection to statistical mechanics: they encode equilibrium physics and enable critical tests of both the eigenstate thermalization hypothesis [12] and random matrix theory predictions [11, 13]. Importantly, thermal states of generic many-body Hamiltonians exhibit highly nontrivial correlations and often volume-law entanglement, making them representative of the “typical” mixed states encountered in quantum chaos and finite-temperature phases [4]. This positions random thermal states as a minimal yet physically grounded ensemble for probing universal many-body phenomena, motivating the development of quantum algorithms that can efficiently generate them without relying on detailed spectral knowledge or classical simulation of the underlying dynamics.

The practical generation of random thermal states remains costly with existing algorithms. Current quantum methods

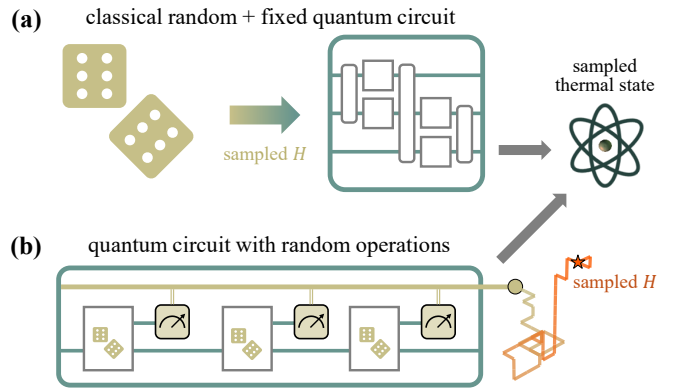


Fig 1. Difference between classical sampling and measurement-controlled sampling. The task is to sample a thermal state together with its Hamiltonian label. (a) Sampling the label via classical computers. The thermal state is prepared using existing thermal-state preparation circuits. (b) Sampling the thermal state and label via one structured random circuit. The label is generated by a random walk based on outcomes of mid-circuit measurements.

typically rely on quantum phase estimation combined with imaginary-time evolution [14–18], fluctuation theorems [19], or quantum Metropolis and Lindbladian thermalization algorithms that couple the system to an effective bath [20–31]. These system-dependent methods are highly effective for preparing one thermal state, but do not directly address the task of sampling thermal states from an ensemble of Hamiltonians. Extending these approaches to generate random thermal states requires repeatedly reconfiguring the algorithm for different Hamiltonian instances, with the randomness largely produced by classical preprocessing steps. The overall pipeline thus lacks global optimization and incurs substantial classical computational overhead, limiting scalability and diminishing the advantages of quantum sampling.

In this letter, we bridge this gap by introducing a dedicated quantum algorithmic framework for the scalable generation

\* felixxinwang@hkust-gz.edu.cn

TABLE I. A comparison of resource complexity requirements to sample a thermal state and its Hamiltonian label  $H$  for different workflows. Here  $n$ ,  $\beta$ ,  $\lambda$ ,  $\epsilon$ , and  $\delta$  denote the number of qubits, inverse temperature, sum of coefficient bounds, target precision, and failure probability.  $t_{\text{mix}}$  denotes the mixing time of a  $\beta$ -dependent Markov chain determined by the sampled  $H$ .

Workflow	Query model	Complexity
Sample label + prepare state	Block encoding of normalized $H$ [16]	$\mathcal{O}\left(2^{n/2}\beta\lambda/\text{Tr}[e^{-\beta H}]\right)$
	Block encoding of jump operators [27]	$\mathcal{O}(\beta t_{\text{mix}})$
Sample state with label	Elementary gates (this work)	$\mathcal{O}\left(n^3\beta^2\epsilon^{-2/3}\log(1/\delta)\right)$

of random thermal states, as illustrated in Figure 1. We assume a setup where the device is programmed solely with a target set of  $L$  Pauli operators  $\Sigma = \{\sigma_1, \dots, \sigma_L\}$  representing the interaction topology. Our protocol autonomously generates the thermal state  $G_{\beta, H} = e^{-\beta H}/\text{Tr}[e^{-\beta H}]$  together with its label  $H = \sum c_j \sigma_j$ , with coefficients  $c_j$  drawn from a random distribution, effectively functioning as a stochastic quantum oracle. This approach bypasses the need for precise deterministic control of every coefficient, instead leveraging the device’s ability to sample from the typical subspace of the Hamiltonian ensemble.

We present our measurement-controlled sampling algorithm as a randomized thermalization process that uses a sequence of thermal-drift channels to generate the thermal ensemble. Compared with existing works [16, 27], we provide the most explicit scaling of the resource complexity with respect to the problem parameters, as shown in Table I. This shift from Hamiltonian-specific preparation to ensemble-based sampling opens new avenues for studying thermal physics at scale. We also analyze the performance of our algorithm in terms of the  $\beta$ -dependence, the resource scaling, and the sampling behaviors through systematic benchmarking experiments. Finally, we apply our algorithm to level-statistic analysis and observe a hallmark of quantum chaos and random matrix universality, distinguishing true quantum scrambling from decoherence or integrable dynamics. The observed Wigner–Dyson universality confirms that our sampler probes genuine many-body chaotic dynamics, connecting quantum algorithms to fundamental questions in random matrix theory. This makes our protocol as a robust tool for both thermodynamic simulation and the verification of quantum advantage.

*Setting.*— We now formalize the sampling task. Given a set of  $L$  linearly independent  $n$ -qubit Pauli words  $\Sigma$  and the inverse temperature  $\beta > 0$ , we denote the ensemble consisting any linear combination of the Pauli’s in  $\Sigma$  with bounded coefficients as,

$$\mathfrak{H} = \left\{ \sum_j c_j \sigma_j : |c_j| \leq h_j, c_j \in \mathbb{R}, \sigma_j \in \Sigma \right\}. \quad (1)$$

where  $h_j$ ’s are the boundary values of the coefficients. The task is to sample from the thermal state  $G_{\beta, H}$  with Hamiltonian  $H$  drawn from the ensemble.

This framework departs from conventional random state

sampling. Standard ensembles, such as Haar random states [32], unitary  $t$ -design [33], or random stabilizer states [34], are typically defined by their geometric properties within the Hilbert space. These ensembles often decouple the state from a specific, physically motivated Hamiltonian. In contrast, our framework asks for generating a structured thermal equilibrium state, explicitly linking the thermodynamics and the random matrix theory. This distinct feature provides a controllable generating set essential for physical benchmarking and Hamiltonian learning.

Our numerical experiments consider two physical ensembles on a  $3 \times 3$  two-dimensional grid, where two-local Pauli operators act on nearest-neighbor pairs. The first is a Heisenberg ensemble with  $\Sigma$  containing operators of the form  $XX$ ,  $YY$ , and  $ZZ$ ; the second is a transverse-field Ising ensemble with  $\Sigma$  containing operators of the form  $ZZ$  and  $X$ . For both ensembles, the coefficient bounds  $h_j$  are uniform, and we denote  $\lambda = \sum_j h_j$ , which upper bounds the largest eigenvalue of any  $H \in \mathfrak{H}$ .

*Quantum thermal-drift channel.*— Ground state preparation is known to be QMA-hard in the worst case [35, 36], and low-temperature thermal state preparation faces comparable complexity barriers [37]. A standard ‘sample-then-prepare’ pipeline, which first selects a Hamiltonian  $H$  and subsequently attempts to prepare its thermal state, is therefore often prohibitively costly. To circumvent this, we implement a randomized thermalization protocol directly on the quantum hardware.

We define the thermal-drift channel  $\mathcal{N}_\sigma$  for any Pauli operator  $\sigma$ , which is the core component of our algorithm. For any input state  $\rho$ , the channel is written in,

$$\mathcal{N}_\sigma(\rho) = \frac{\mu}{2} (|\uparrow\rangle\langle\uparrow| \otimes \mathcal{E}_\sigma^\uparrow(\rho) + |\downarrow\rangle\langle\downarrow| \otimes \mathcal{E}_\sigma^\downarrow(\rho)), \quad (2)$$

where  $\mu < 1$  is a scaling factor. Here, for any state  $\rho$ , the maps  $\mathcal{E}_\sigma^\uparrow$  and  $\mathcal{E}_\sigma^\downarrow$  are two completely positive and non-trace-preserving operations defined as  $e^{+\tau\sigma/2}\rho e^{+\tau\sigma/2}$  and  $e^{-\tau\sigma/2}\rho e^{-\tau\sigma/2}$ , respectively, with a thermal strength  $\tau > 0$ . The first register of  $\mathcal{N}_\sigma(\rho)$  naturally generates a random branch. Measuring this flag register indicates which direction the state is thermalized toward, with probabilities proportional to the corresponding unnormalized traces.

The thermal-drift channel can be implemented using system-ancilla coupling in a dilated Hilbert space, followed by measuring and tracing out the flag register. In particular, we consider the following map

$$\mathcal{N}_{\approx}(\rho) = \frac{1}{1+\mu} \mathcal{N}_\sigma(\rho) + \frac{\mu}{1+\mu} |\circlearrowleft\rangle\langle\circlearrowleft| \otimes \rho, \quad (3)$$

where  $|\uparrow\rangle$ ,  $|\downarrow\rangle$  and  $|\circlearrowleft\rangle$  are mutually orthogonal states. This map can be implemented within  $\mathcal{O}(n)$  quantum elementary gates and  $2n$  ancilla qubits. Then, with failure probability at most  $\delta$ , the thermal-drift channel is simulated by repeatedly applying  $\mathcal{N}_{\approx}$  and the associated measure-and-trace operations until the measurement outcome is not ‘ $\circlearrowleft$ ’, using at most  $\log(1/\delta)$  repetitions. In particular, the same state and ancillas can be reused without postselection. We refer to the Supplementary Material for a detailed implementation.

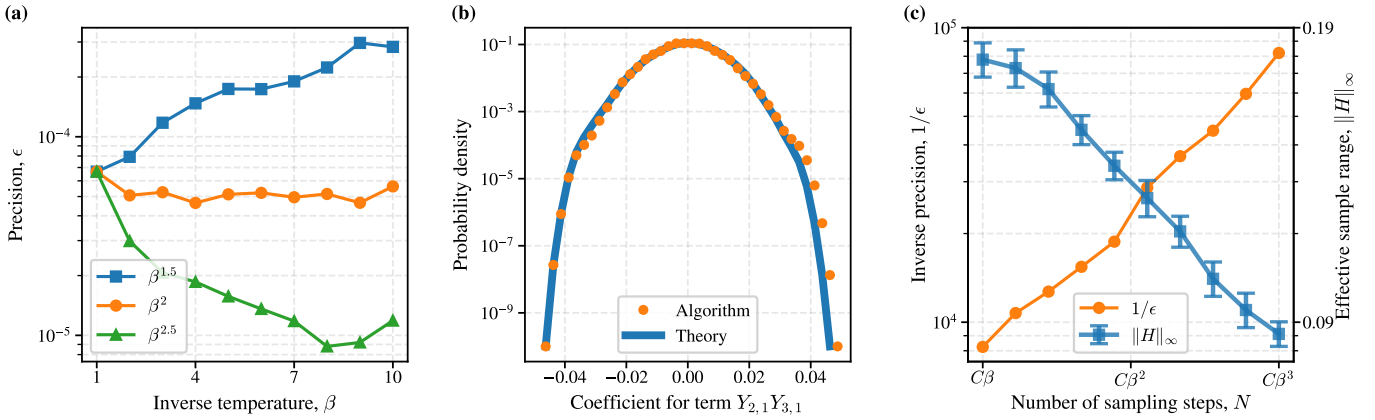


Fig 2. Numerical verification of the theoretical predictions for the thermal-drift sampling algorithm applied to a  $3 \times 3$  two-dimensional Heisenberg model. (a) Precision  $\epsilon$  between the output state and the ideal thermal state as a function of the inverse temperature  $\beta$ , for different step scalings. (b) Empirical marginal distribution of a nearest-neighbor  $YY$  interaction coefficient, compared with the theoretical prediction from Theorem 2. Here  $Y_{i,j}$  denotes the Pauli- $Y$  operator on the site at row  $i$  and column  $j$ . (c) Trade-off between inverse precision and effective sample range at fixed  $\beta$ , as the number of steps  $N$  increases from  $C\beta$  to  $C\beta^3$ , where  $C$  is a fixed constant. See the Supplementary Material for more experimental details.

*Algorithm overview.*— We now present the thermal state sampling algorithm, implemented as a circuit of  $N$  blocks applied to an initial state  $\rho_0$ . In block  $k$ , a thermal-drift channel  $\mathcal{N}_{\sigma_{j_k}}$  is applied, where  $\sigma_{j_k}$  is selected independently from the set  $\Sigma$ . The probability of choosing  $\mathcal{N}_{\sigma_j}$  is weighted by the bound  $h_j$ , so that the distribution is  $h_j/\lambda$ . The thermal strength is fixed across all blocks to  $\tau = \beta\lambda/N$ . After the thermal-drift channel, a measure-and-trace operation  $\mathcal{M}_{m_k}$  is applied to the flag register, generating a measurement outcome  $m_k$ . This outcome is recorded as  $m_k \in \{+1, -1\}$  corresponding to  $\uparrow$  and  $\downarrow$ .

The full circuit implementation is labeled by an ordered list of values  $\mathbf{j} = \{j_1, \dots, j_N\}$  and an ordered list of directions  $\mathbf{m} = \{m_1, \dots, m_N\}$ , that corresponds to the channel

$$\mathcal{E}_{\mathbf{j}, \mathbf{m}} = \mathcal{M}_{m_N} \circ \mathcal{N}_{\sigma_{j_N}} \circ \dots \circ \mathcal{M}_{m_1} \circ \mathcal{N}_{\sigma_{j_1}}. \quad (4)$$

In particular, one can collect the accumulated drift along each Pauli axis  $\sigma_j$ , which defines the overall Hamiltonian label

$$H_{\mathbf{j}, \mathbf{m}} = \frac{\lambda}{N} \sum_{j=1}^N \sum_{k: j_k=j} m_k \sigma_j. \quad (5)$$

This Hamiltonian can be understood as the label associated with the operation that maps the initial state  $\rho_0$  to the output state  $\mathcal{E}_{\mathbf{j}, \mathbf{m}}(\rho_0)$ . When  $\rho_0$  is the maximally mixed state, the output state is then a copy of its thermal state

$$\mathcal{E}_{\mathbf{j}, \mathbf{m}}(\rho_0) \approx G_{\beta, H_{\mathbf{j}, \mathbf{m}}}. \quad (6)$$

Finally, sampling indices with weights  $h_j/\lambda$  controls the effective coefficient scales, so that the induced labels conform to the envelope specified by  $h$ , thereby completing the task of thermal state sampling.

*Sampling error and distribution.*— Unlike randomized algorithms such as qDRIFT [38], where the randomness is Markovian and can be analyzed directly in channel form, each

measurement outcome in our algorithm depends on the evolving state, and hence the process is generally non-Markovian. We therefore use probabilistic tools to analyze the sampling error and the induced distribution over labels.

We start with the sampling error  $\epsilon$ , quantified by the trace distance between the output state of our algorithm and the ideal thermal state of the sampled Hamiltonian. Given the sampled outcomes  $\mathbf{j}$  and  $\mathbf{m}$ , we consider the effective Hamiltonian  $H_{\approx}$  such that  $\mathcal{E}_{\mathbf{j}, \mathbf{m}}(\rho_0) = e^{-\beta H_{\approx}} / \text{Tr}[e^{-\beta H_{\approx}}]$ . Then the sampling error is bounded by  $\epsilon \leq \beta \|H_{\mathbf{j}, \mathbf{m}} - H_{\approx}\|_{\infty}$ . When the number of steps  $N$  is not large enough so that most sampled Pauli operators are distinct, the sampling error behaves like the discretization error of a second-order Trotter product formula, scaling as  $\mathcal{O}(\beta^3)$  [39]. However, when  $N$  is sufficiently large so that Pauli operators are likely repetitive, we treat  $\mathbf{m}$  as random variables conditional on a fixed  $\mathbf{j}$ . In this regime, the Freedman inequality for matrix martingales [40] implies an  $\mathcal{O}(\beta^2)$  scaling almost surely. This leads to the following.

**Theorem 1** *For any system size  $n$ , inverse temperature  $\beta$ , and sufficiently large  $N$ , our algorithm uses  $\mathcal{O}(nN \log(1/\delta))$  gates to sample a thermal state and its label, with precision  $\tilde{\mathcal{O}}(n^{3/2} \lambda^3 \beta^3 N^{-3/2})$  and failure probability at most  $\delta$ .*

Here  $\tilde{\mathcal{O}}(\cdot)$  omits the logarithm terms. Theorem 1 is numerically verified in Figure 2(a). For increasing inverse temperature starting at  $\beta = 1$ , we test our algorithm with number of steps  $N = \mathcal{O}(\beta^k)$  for  $k = 1.5, 2$  and  $2.5$ , and observe that the average trace-distance error scales as  $\mathcal{O}(\beta^{2-k})$ , consistent with Theorem 1. Unless extra clarified, we take  $N = n^2 \beta^2 \epsilon^{-2/3}$  in the rest of experiments.

To obtain a theoretical analysis of the sample distribution, we consider an asymptotic regime where the number of sampling steps  $N$  tends to infinity, so that every possible label  $H \in \mathfrak{H}$  can be sampled. Then our algorithm can be modeled

as a random walk  $(\mathbf{x}^{(k)})_k$  on an  $L$ -dimensional integer lattice  $\mathbb{Z}^L$ , such that  $\mathbf{x}^{(0)}$  and  $\mathbf{x}^{(N)}$  correspond to the identity matrix and the sampled label  $H$ , respectively. Such a walk sequence satisfies for all  $k \geq 1$ ,

$$\Pr(\mathbf{x}^{(k)} - \mathbf{x}^{(k-1)} = \pm e_j) = \Pr(m_k = \pm 1) \cdot h_j/\lambda, \quad (7)$$

where  $e_j$  denotes the  $j$ -th unit vector. Applying lattice-based random walk theory [41] yields a Gaussian approximation to the endpoint distribution under appropriate scaling. Combined with the thermal reweighting from  $\Pr(m_k = \pm 1)$ , the sampling rule takes a product form involving the partition function and a normal density.

**Theorem 2** For any inverse temperature  $\beta$ , a label  $H \in \mathfrak{H}$  can be asymptotically sampled by our algorithm with probability proportional to  $\text{Tr}[e^{-\beta H}] D(\mathbf{x})$ , where  $D$  is an  $L$ -dimensional multivariate normal distribution and  $\mathbf{x}$  satisfies  $\mathbf{x}_j = \text{Tr}[H\sigma_j]/\lambda \cdot N$ .

We numerically show that a similar result holds in non-asymptotic cases. Taking  $\beta = 2$ , we sample from our algorithm and visualize one-dimensional slices of the marginal distribution of a chosen Pauli coefficient. As shown in Figure 2(b), the empirical distribution closely matches the ideal one. Note that the difference mainly occurs in both ends of the distribution, which will get smaller as the number of sampling step further increases.

Theorems 1 and 2 together imply a trade-off between sample accuracy and effective sample range. Due to the nature of random walks, higher accuracy comes with a more concentrated label distribution, and vice versa. As shown in Figure 2(c), for  $\beta = 2$ , as the number of steps  $N$  increases from  $\mathcal{O}(\beta)$  to  $\mathcal{O}(\beta^3)$ , the inverse precision  $1/\epsilon$  increases while the effective sample range  $\|H\|_\infty$  decreases at a similar rate. Therefore, despite the efficiency of a single execution, it is not recommended to use our algorithm for preparing thermal states of one fixed Hamiltonian. However, this characteristic makes our algorithm particularly well-suited for ensemble-level applications.

*Application to the level statistics.*— A natural application of our thermal state sampler is level statistics, which characterizes thermodynamic phases in quantum many-body systems [42]. Given any random density operator with an ordered many-body eigenvalue spectrum  $\{\lambda_j\}$ , one defines the adjacent logarithmic level spacings  $\delta_j = \log(\lambda_j/\lambda_{j+1})$  and the dimensionless spacing (gap) ratio [43, 44],

$$r_j = \frac{\min\{\delta_j, \delta_{j+1}\}}{\max\{\delta_j, \delta_{j+1}\}} \in [0, 1], \quad (8)$$

whose distribution is insensitive to spectral unfolding and thus widely used in finite-size studies [10, 13, 45]. In ergodic systems satisfying the eigenstate thermalization hypothesis, strong level repulsion leads to Wigner–Dyson statistics [13, 46], whereas in the many-body localization phase, emergent local integrals of motion suppress correlations and produce Poisson level statistics [11, 47]. The gap ratio and

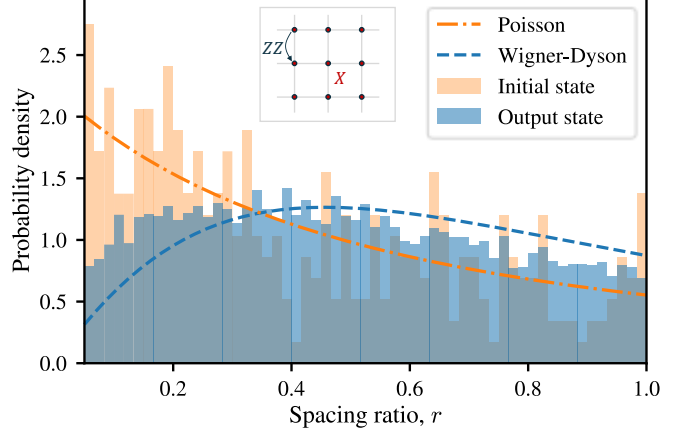


Fig 3. Level-spacing ratio statistics of the sampled thermal states for a  $3 \times 3$  2D transverse-field Ising model. Shown is the distribution of the adjacent level-spacing ratio  $r$ . The orange histogram in the background corresponds to the initial state, while the blue histogram in the foreground corresponds to the output state generated by the sampling algorithm. The blue dashed curve indicates the Wigner–Dyson prediction, and the orange dash-dotted curve indicates the Poisson prediction. See the Supplementary Material for additional experimental details.

disorder-averaged  $\langle r \rangle$  therefore provide a clear diagnostic of the crossover or transition between these regimes [45, 48].

We further apply our framework as a diagnostic tool to assess the chaotic nature of the generated states. In particular, we apply our algorithm to investigate the level statistics of the generated thermal state ensemble. We compare an initial reference state whose spectrum exhibits near-Poisson statistics with the output states produced by our sampling algorithm. As shown in Figure 3, aggregating  $\{r_j\}$  over samples yields a robust, unfolding-free diagnostic. The analysis uncovers a clear signature of thermalization that the level statistics shift from a Poissonian distribution in the reference state to a Wigner–Dyson distribution in the output ensemble. This observation indicates that the sampler accesses a substantially more chaotic sector of Hilbert space than the structured input, consistent with the interpretation that the generated states are not efficiently captured by simple classical models.

*Conclusion and outlook.*— We have developed a method to efficiently generate random thermal states for Hamiltonians drawn from broad Pauli ensembles, which opens several directions. On the physics side, our method provides direct access to level statistics, entanglement measures, and finite-temperature signatures without reliance on exact diagonalization or classical Monte Carlo methods [20]. On the computation side, our method generates thermal randomness in comparison to Haar randomness for benchmarking quantum devices. More broadly, our results suggest a shift from Hamiltonian-specific thermalization protocols toward measurement-controlled ensemble sampling, with potential implications for quantum simulation in sign-problem-limited regimes and for quantum machine learning, where thermal states serve as training data and their Hamiltonian labels enable supervised learning of many-body properties [14,

[49, 50]. Our framework integrates quantum algorithms, statistical mechanics, and machine learning, providing tools for both near-term quantum applications and fundamental many-body physics. We expect these directions to further clarify the role of randomness, temperature, and complexity in interacting quantum systems.

*Note added.*— In the final stages of preparing this manuscript, the authors became aware of independent works [51, 52] that also generate thermal states by applying sequences of Pauli-based nonunitary updates, typically starting from the maximally mixed state. These works focus on thermal-state preparation for a given Hamiltonian via classical algorithms, whereas we focus on sampling from a thermal ensemble that outputs a thermal state together with its Hamiltonian via quantum circuits.

*Acknowledgment.*— The authors are listed in alphabetical order. This work was partially supported by the National Key R&D Program of China (Grant No. 2024YFB4504004), the National Natural Science Foundation of China (Grant No. 12447107, 92576114), the Guangdong Provincial Quantum Science Strategic Initiative (Grant No. GDZX2403008, GDZX2503001), the CCF-Tencent Rhino-Bird Open Research Fund, and the Guangdong Provincial Key Lab of Integrated Communication, Sensing and Computation for Ubiquitous Internet of Things (Grant No. 2023B1212010007).

*Code availability.*— Numerical experiments are based on an open-source Python research software for quantum computing [53]. Code and data used in the numerical experiments are available on <https://github.com/QuAIR/SamplingThermalState-Codes>.

---

[1] Jonas Maziero. Random sampling of quantum states: A survey of methods. *Braz. J. Phys.*, 45(6):575–583, 2015.

[2] Joonhee Choi, Adam L. Shaw, Ivaylo S. Madjarov, Xin Xie, Ran Finkelstein, Jacob P. Covey, Jordan S. Cotler, Daniel K. Mark, Hsin-Yuan Huang, Anant Kale, Hannes Pichler, Fernando G. S. L. Brandão, Soonwon Choi, and Manuel Endres. Preparing random states and benchmarking with many-body quantum chaos. *Nature*, 613(7944):468–473, 2023.

[3] M. Oszmaniec, R. Augusiak, C. Gogolin, J. Kołodyński, A. Acín, and M. Lewenstein. Random bosonic states for robust quantum metrology. *Phys. Rev. X*, 6:041044, 2016.

[4] Tong Liu, Shang Liu, Hekang Li, Hao Li, Kaixuan Huang, Zhongcheng Xiang, Xiaohui Song, Kai Xu, Dongning Zheng, and Heng Fan. Observation of entanglement transition of pseudo-random mixed states. *Nat. Commun.*, 14(1):1971, 2023.

[5] Easwar Magesan, J. M. Gambetta, and Joseph Emerson. Scalable and robust randomized benchmarking of quantum processes. *Phys. Rev. Lett.*, 106(18):180504, 2011.

[6] Patrick Hayden and John Preskill. Black holes as mirrors: quantum information in random subsystems. *J. High Energy Phys.*, 2007(09):120, 2007.

[7] Frank Arute, Kunal Arya, Ryan Babbush, and et. al. Quantum supremacy using a programmable superconducting processor. *Nature*, 574(7779):505–510, 2019.

[8] Sergio Boixo, Sergei V. Isakov, Vadim N. Smelyanskiy, Ryan Babbush, Nan Ding, Zhang Jiang, Michael J. Bremner, John M. Martinis, and Hartmut Neven. Characterizing quantum supremacy in near-term devices. *Nat. Phys.*, 14(6):595–600, 2018.

[9] Christoph Dankert, Richard Cleve, Joseph Emerson, and Etera Livine. Exact and approximate unitary 2-designs and their application to fidelity estimation. *Phys. Rev. A*, 80:012304, 2009.

[10] J. Odavić, G. Torre, N. Mićić, D. Davidović, F. Franchini, and S. M. Giampaolo. Random unitaries, robustness, and complexity of entanglement. *Quantum*, 7:1115, 2023.

[11] Vedika Khemani, S. P. Lim, D. N. Sheng, and David A. Huse. Critical properties of the many-body localization transition. *Phys. Rev. X*, 7(2):021013, 2017.

[12] Luca D’Alessio, Yariv Kafri, Anatoli Polkovnikov, and Marcos Rigol. From quantum chaos and eigenstate thermalization to statistical mechanics and thermodynamics. *Adv. Phys.*, 65(3):239–362, 2016.

[13] Wouter Buijsman, Vadim Cheianov, and Vladimir Gritsev. Random matrix ensemble for the level statistics of many-body localization. *Phys. Rev. Lett.*, 122(18):180601, 2019.

[14] David Poulin and Paweł Wocjan. Sampling from the thermal quantum Gibbs state and evaluating partition functions with a quantum computer. *Phys. Rev. Lett.*, 103:220502, 2009.

[15] Anirban Narayan Chowdhury and Rolando D. Somma. Quantum algorithms for Gibbs sampling and hitting-time estimation. *Quantum Inf. Comput.*, 17(1–2):41–64, 2017.

[16] András Gilyén, Yuan Su, Guang Hao Low, and Nathan Wiebe. Quantum singular value transformation and beyond: Exponential improvements for quantum matrix arithmetics. In *Proceedings of the 51st Annual ACM SIGACT Symposium on Theory of Computing*, STOC 2019, page 193–204, New York, NY, USA, 2019. Association for Computing Machinery.

[17] Mario Motta, Chong Sun, Adrian T. K. Tan, Matthew J. O’Rourke, Erika Ye, Austin J. Minich, Fernando G. S. L. Brandão, and Garnet Kin-Lic Chan. Determining eigenstates and thermal states on a quantum computer using quantum imaginary time evolution. *Nat. Phys.*, 16(2):205–210, 2020.

[18] Cambaye Rouzé, Daniel Stilck França, and Álvaro M. Alhambra. Optimal quantum algorithm for Gibbs state preparation, 2024.

[19] Zoe Holmes, Gopikrishnan Muraleedharan, Rolando D. Somma, Yigit Subasi, and Burak Şahinoğlu. Quantum algorithms from fluctuation theorems: Thermal-state preparation. *Quantum*, 6:825, 2022.

[20] Kristan Temme, Tobias J. Osborne, Karl G. Vollbrecht, David Poulin, and Frank Verstraete. Quantum Metropolis sampling. *Nature*, 471(7336):87–90, 2011.

[21] Man-Hong Yung and Alán Aspuru-Guzik. A quantum-quantum Metropolis algorithm. *Proc. Natl. Acad. Sci. U.S.A.*, 109(3):754–759, 2012.

[22] Jonathan E. Moussa. Low-depth quantum Metropolis algorithm, 2022.

[23] Patrick Rall, Chunhao Wang, and Paweł Wocjan. Thermal state preparation via rounding promises. *Quantum*, 7:1132, 2023.

[24] Oles Shtanko and Ramis Movassagh. Preparing thermal states on noiseless and noisy programmable quantum processors, 2023.

[25] Paweł Wocjan and Kristan Temme. Szegedy walk unitaries for quantum maps. *Commun. Math. Phys.*, 402(3):3201–3231, 2023.

[26] Chi-Fang Chen, Michael J. Kastoryano, Fernando G. S. L. Brandão, and András Gilyén. Quantum thermal state preparation, 2023.

[27] Chi-Fang Chen, Michael J. Kastoryano, and András Gilyén. An efficient and exact noncommutative quantum Gibbs sampler, 2025.

[28] Chi-Fang Chen, Michael Kastoryano, Fernando G. S. L. Brandão, and András Gilyén. Efficient quantum thermal simulation. *Nature*, 646(8085):561–566, 2025.

[29] Zhiyan Ding, Bowen Li, and Lin Lin. Efficient quantum Gibbs samplers with Kubo–Martin–Schwinger detailed balance condition. *Commun. Math. Phys.*, 406(3):67, 2025.

[30] Daniel Zhang, Jan Lukas Bosse, and Toby Cubitt. Dissipative quantum Gibbs sampling, 2023.

[31] Fernando G. S. L. Brandão and Michael J. Kastoryano. Finite correlation length implies efficient preparation of quantum thermal states. *Commun. Math. Phys.*, 365(1):1–16, 2019.

[32] Zhengfeng Ji, Yi-Kai Liu, and Fang Song. Pseudorandom quantum states. In *Annual International Cryptology Conference*, pages 126–152. Springer, 2018.

[33] Joseph Emerson, Yaakov S Weinstein, Marcos Saraceno, Seth Lloyd, and David G Cory. Pseudo-random unitary operators for quantum information processing. *science*, 302(5653):2098–2100, 2003.

[34] Héctor J García, Igor L Markov, and Andrew W Cross. On the geometry of stabilizer states. *arXiv preprint arXiv:1711.07848*, 2017.

[35] John Watrous. *Quantum Computational Complexity*, pages 7174–7201. Springer New York, New York, NY, 2009.

[36] Anirban N. Chowdhury, Guang Hao Low, and Nathan Wiebe. A variational quantum algorithm for preparing quantum Gibbs states, 2020.

[37] Dorit Aharonov, Itai Arad, and Thomas Vidick. The quantum PCP conjecture, 2013.

[38] Earl Campbell. Random compiler for fast Hamiltonian simulation. *Phys. Rev. Lett.*, 123(7):070503, 2019.

[39] Andrew M. Childs, Dmitri Maslov, Yunseong Nam, Neil J. Ross, and Yuan Su. Toward the first quantum simulation with quantum speedup. *Proc. Natl. Acad. Sci. U.S.A.*, 115(38):9456–9461, 2018.

[40] Joel A. Tropp. Freedman’s inequality for matrix martingales. *Electron. Commun. Probab.*, 16:262–270, 2011.

[41] Frank Spitzer. *Principles of random walk*. Springer, New York, NY, 2001.

[42] Andrew C. Potter, Romain Vasseur, and S. A. Parameswaran. Universal properties of many-body delocalization transitions. *Phys. Rev. X*, 5(3):031033, 2015.

[43] Vadim Oganesyan and David A. Huse. Localization of interacting Fermions at high temperature. *Phys. Rev. B*, 75:155111, 2007.

[44] Piotr Sierant and Jakub Zakrzewski. Model of level statistics for disordered interacting quantum many-body systems. *Phys. Rev. B*, 101(10):104201, 2020.

[45] Maksym Serbyn and Joel E. Moore. Spectral statistics across the many-body localization transition. *Phys. Rev. B*, 93(4):041424, 2016.

[46] Eugene P Wigner. Random matrices in physics. *SIAM review*, 9(1):1–23, 1967.

[47] Arijeet Pal and David A. Huse. Many-body localization phase transition. *Phys. Rev. B*, 82(17):174411, 2010.

[48] D. A. Rabson, B. N. Narozhny, and A. J. Millis. Crossover from Poisson to Wigner–Dyson level statistics in spin chains with integrability breaking. *Phys. Rev. B*, 69(5):054403, 2004.

[49] Hsin-Yuan Huang, Michael Broughton, Masoud Mohseni, Ryan Babbush, Sergio Boixo, Hartmut Neven, and Jarrod R McClean. Power of data in quantum machine learning. *Nat. Commun.*, 12(1):2631, 2021.

[50] Seth Lloyd and Christian Weedbrook. Quantum generative adversarial learning. *Phys. Rev. Lett.*, 121:040502, 2018.

[51] Rafael Gómez-Lurbe and Armando Pérez. Pauli propagation for imaginary time evolution. *arXiv preprint arXiv:2601.14400*, 2026.

[52] Manuel S. Rudolph, Armando Angrisani, Andrew Wright, Iwo Sanderski, Ricard Puig, and Zoë Holmes. Thermal state simulation with pauli and majorana propagation, February 2026.

[53] QuAIR team. QuAIRKit. <https://github.com/QuAIR/QuAIRKit>, 2023.

[54] Nicholas J. Higham. *Functions of Matrices*. Society for Industrial and Applied Mathematics, Philadelphia, PA, 2008.

[55] Rajendra Bhatia and Hideki Kosaki. Mean matrices and infinite divisibility. *Linear Algebra Appl.*, 424(1):36–54, 2007. Special Issue in honor of Roger Horn.

[56] Roger A. Horn and Charles R. Johnson. *Matrix analysis*, 2nd Edition. Cambridge University Press, Cambridge, United Kingdom, 2012.

[57] Brian C. Hall. *Lie Groups, Lie Algebras, and Representations: An Elementary Introduction*. Springer, New York, US, 2015.

[58] Y. Y. Atas, E. Bogomolny, O. Giraud, and G. Roux. Distribution of the ratio of consecutive level spacings in random matrix ensembles. *Physical Review Letters*, 110(8):084101, February 2013.

# Appendix for

## Thermal-Drift Sampling: Generating Random Thermal Ensembles for Quantum Chaos Diagnostics

### Appendix A: Preliminaries

#### 1. Notations

*Asymptotic notations.* Let  $[N] = \{1, 2, \dots, N\}$  for any positive integer  $N$ . We use asymptotic notations to describe the scaling of complexity and error bounds. For two non-negative functions  $f(x)$  and  $g(x)$ , we write  $f(x) = \mathcal{O}(g(x))$  if there exist constants  $C > 0$  and  $x_0$  such that  $f(x) \leq Cg(x)$  for all  $x \geq x_0$ . Conversely,  $f(x) = \Omega(g(x))$  indicates that  $f(x) \geq cg(x)$  for some constant  $c > 0$  and sufficiently large  $x$ . The notation  $f(x) = o(g(x))$  implies that  $\lim_{x \rightarrow \infty} f(x)/g(x) = 0$ . We also use the soft-O notation  $\tilde{\mathcal{O}}(g(x))$  to suppress polylogarithmic factors, i.e.,  $\tilde{\mathcal{O}}(g(x)) \equiv \mathcal{O}(g(x) \text{poly}(\log g(x)))$ .

*Operators.* We denote the single-qubit Pauli operators by the set  $\{I, X, Y, Z\}$ , defined as  $I = \begin{pmatrix} 1 & 0 \\ 0 & 1 \end{pmatrix}$ ,  $X = \begin{pmatrix} 0 & 1 \\ 1 & 0 \end{pmatrix}$ ,  $Y = \begin{pmatrix} 0 & -i \\ i & 0 \end{pmatrix}$  and  $Z = \begin{pmatrix} 1 & 0 \\ 0 & -1 \end{pmatrix}$ . The set of  $n$ -qubit Pauli operators is denoted as  $\{I, X, Y, Z\}^{\otimes n}$ . We denote the Hadamard gate and the single-qubit rotation around the  $y$ -axis by:  $H = \frac{1}{\sqrt{2}} \begin{pmatrix} 1 & 1 \\ 1 & -1 \end{pmatrix}$  and  $R_y(\theta) = e^{-i\theta Y/2} = \begin{pmatrix} \cos(\theta/2) & -\sin(\theta/2) \\ \sin(\theta/2) & \cos(\theta/2) \end{pmatrix}$ . The commutator of operators  $A$  and  $B$  is  $[A, B] = AB - BA$ . The adjoint action (Lie bracket) is defined recursively as  $\text{ad}_A(B) = [A, B]$  and  $\text{ad}_A^k(B) = [A, \text{ad}_A^{k-1}(B)]$  for  $k \geq 2$ .

*Quantum systems.* Let  $\mathcal{H}$  denote a finite-dimensional complex Hilbert space. A density operator  $\rho \in \mathcal{H}$  is positive semi-definite with unit trace, and we write  $\mathcal{D}(\mathcal{H}_A)$  for the set of density operators on a system  $A$  with Hilbert space  $\mathcal{H}_A$ . For a composite system with Hilbert space  $\mathcal{H}_{AB} = \mathcal{H}_A \otimes \mathcal{H}_B$ , we write  $X_A \equiv X \otimes I_B$  to denote an operator  $X$  acting locally on subsystem  $A$ , where  $I_B$  is the identity on  $\mathcal{H}_B$ .

*Norms.* For a vector  $\mathbf{x} = (\mathbf{x}_1, \dots, \mathbf{x}_L) \in \mathbb{C}^L$ , we define the Euclidean norm as  $\|\mathbf{x}\| = \sqrt{\sum_{i=1}^L |\mathbf{x}_i|^2}$ . For a matrix  $A \in \mathbb{C}^{d \times d}$ , we define the spectral norm  $\|A\|_\infty$  as the largest singular value of  $A$ , and the trace norm  $\|A\|_1$  as the sum of the singular values of  $A$ .

*Parity functions.* For  $N \in \mathbb{N}$  and  $\mathbf{x} = (\mathbf{x}_1, \dots, \mathbf{x}_L) \in \mathbb{Z}^L$ , define the *reachability parity function*  $a_N : \mathbb{Z}^L \rightarrow \{0, 2\}$  by

$$a_N(\mathbf{x}) = \begin{cases} 2, & \text{if } \sum_{j=1}^L |\mathbf{x}_j| \leq N \text{ and } N - \sum_{j=1}^L |\mathbf{x}_j| \text{ is even;} \\ 0, & \text{otherwise.} \end{cases} \quad (\text{S1})$$

Thus  $a_N(\mathbf{x}) = 0$  whenever  $\mathbf{x}$  is not reachable from the origin in  $N$  steps of the walk, and  $a_N(\mathbf{x}) = 2$  otherwise. Define the *bitwise parity function* for  $x \in \mathbb{N}$  as

$$p(x) = \begin{cases} 0, & \text{if } \sum_i x_i \text{ is even;} \\ 1, & \text{otherwise,} \end{cases} \quad (\text{S2})$$

where  $x_{N-1} \cdots x_0$  is the binary representation of  $x = \sum_i 2^i x_i$ . Denote the first  $l-1$  bits of  $x$  as  $x_{1:l} := x_1 \cdots x_{l-1}$ .

*Martingales.* A *filtration* is a sequence of  $\sigma$ -algebras  $\{\mathcal{F}_0, \mathcal{F}_1, \dots\}$  satisfying  $\mathcal{F}_0 \subseteq \mathcal{F}_1 \subseteq \dots$ . A sequence of random variables  $\{X_k\}_{k \geq 0}$  is a *martingale* with respect to  $\{\mathcal{F}_k\}$  if  $X_k$  is  $\mathcal{F}_k$ -measurable,  $\mathbb{E}[|X_k|] < \infty$ , and  $\mathbb{E}[X_{k+1} | \mathcal{F}_k] = X_k$ . A sequence  $\{Y_k\}_{k \geq 1}$  is a *martingale difference sequence* (MDS) if it is adapted to the filtration and satisfies  $\mathbb{E}[Y_{k+1} | \mathcal{F}_k] = 0$ . An MDS is typically constructed from a martingale  $\{X_k\}_k$  by setting  $Y_k = X_k - X_{k-1}$ .

#### 2. Useful lemmas

This section collects auxiliary lemmas used in later proofs.

**Lemma S1 (Fr  ochet derivative of matrix exponential, [54])** *Let  $A, E$  be two matrices. Then*

$$\frac{d}{dt} e^{A+tE} = \int_0^1 e^{s(A+tE)} E e^{(1-s)(A+tE)} ds. \quad (\text{S3})$$

**Lemma S2** For any Hermitian matrix  $X$  and positive semidefinite matrix  $R$ ,

$$\left\| \int_0^1 R^s X R^{1-s} ds \right\|_1 \leq \|X\|_\infty \|R\|_1 \quad (\text{S4})$$

**Proof** Suppose  $R$  has the spectral decomposition  $R = UDU^\dagger = \sum_j p_j |j\rangle\langle j|$  for some orthonormal basis  $\{|j\rangle\}_j$ . Denote  $\mathcal{L}(X) = \int_0^1 D^s X D^{1-s} ds$ . Consider the  $(i, j)$ th element of  $\mathcal{L}(X)$ :

$$\langle i | \mathcal{L}(X) | j \rangle = \langle i | \int_0^1 \sum_k p_k^s |k\rangle\langle k| X \sum_{k'} p_{k'}^{1-s} |k'\rangle\langle k'| ds |j\rangle \quad (\text{S5})$$

$$= \langle i | X | j \rangle \int_0^1 p_i^s p_j^{1-s} ds \quad (\text{S6})$$

$$= X_{i,j} L(p_i, p_j), \quad (\text{S7})$$

where

$$L(a, b) = \begin{cases} a, & \text{if } a = b; \\ \frac{a-b}{\log a - \log b}, & \text{if } a \neq b. \end{cases} \quad (\text{S8})$$

Denote the  $(i, j)$ th element of matrix  $\mathcal{L}$  as  $L(p_i, p_j)$ . The matrix  $\mathcal{L}$  is the Loewner matrix of the Schlicht function  $\log z$  mapping the upper half-plane into itself [55], so  $\mathcal{L}$  is positive semidefinite (PSD). Since  $\mathcal{L}(X) = X \odot \mathcal{L}$ , where  $\odot$  is the Hadamard product, the Schur product theorem [56, Section 7.5] implies that  $\mathcal{L}(X)$  is PSD whenever  $X$  is PSD. Therefore,

$$\mathcal{L}(\|X\|_\infty I) = \|X\|_\infty D \succeq \mathcal{L}(X) \succeq -\|X\|_\infty D = \mathcal{L}(-\|X\|_\infty I). \quad (\text{S9})$$

Denote  $\lambda_1(X), \lambda_2(X), \dots$  as the eigenvalues of  $X$  in ascending order.  $\mathcal{L}(X) \succeq -\|X\|_\infty D$  means  $-\lambda_j(\mathcal{L}(X)) \leq \|X\|_\infty \lambda_j(D)$  for all  $j$  satisfying  $\lambda_j(\mathcal{L}(X)) < 0$ , while  $\|X\|_\infty D \succeq \mathcal{L}(X)$  means  $\lambda_j(\mathcal{L}(X)) \leq \|X\|_\infty \lambda_j(D)$  for all  $j$  satisfying  $\lambda_j(\mathcal{L}(X)) \geq 0$ . Combining, we have

$$\|\mathcal{L}(X)\|_1 = \sum_j |\lambda_j(\mathcal{L}(X))| \leq \|X\|_\infty \sum_j \lambda_j(D) = \|X\|_\infty \|D\|_1 = \|X\|_\infty \|R\|_1. \quad (\text{S10})$$

■

**Lemma S3 (Baker–Campbell–Hausdorff formula for  $e^X e^Y e^X$ , [57])** For matrices  $X$  and  $Y$ ,

$$\log(e^X e^Y e^X) = 2X + Y - \frac{1}{6} [X + Y, [X, Y]] + \mathcal{O}((\|X\|_\infty + \|Y\|_\infty)^5). \quad (\text{S11})$$

**Lemma S4 (Freedman Inequality for Hermitian matrices, [40])** Let  $(\mathcal{F}_k)_k$  be a filtration, and let  $(X_k)_k$  be a martingale difference sequence of  $d$ -dimensional Hermitian matrices such that  $\|X_k\|_\infty \leq R$  for some  $R > 0$ . Then the partial sum  $Y_k = \sum_{i=1}^k X_i$  and the predictable quadratic variation process  $W_k = \sum_{i=1}^k \mathbb{E}[X_i^2 | \mathcal{F}_{i-1}]$  satisfies for all  $t \geq 0$  and  $\sigma^2 > 0$ ,

$$\Pr(\exists k > 0 : \|Y_k\|_\infty > t \text{ and } \|W_k\|_\infty \leq \sigma^2) \leq 2d \exp\left(-\frac{t^2/2}{\sigma^2 + Rt/3}\right). \quad (\text{S12})$$

**Lemma S5 (Lattice-based random walk, [41])** Consider a random walk  $(\mathbf{x}^{(k)})_k$  on a lattice  $\{-N, \dots, N\}^{\times L}$  with  $\mathbf{x}^{(0)} = 0$ , and there exists  $p_1, \dots, p_L$  such that for all  $j$  and  $k$ ,  $\Pr(\mathbf{x}^{(k)} - \mathbf{x}^{(k-1)} = \pm e_j) = p_j/2$ . Then for any endpoint  $\mathbf{x} \in \mathbb{Z}^L$  such that  $\sum_j \mathbf{x}_j^2 = N$ ,

$$\Pr_Q(\mathbf{x}^{(N)} = \mathbf{x}) = \frac{a_N(\mathbf{x})}{(2\pi N)^{L/2} \sqrt{\prod_{j=1}^L p_j}} \exp\left(-\frac{1}{2N} \sum_j \frac{\mathbf{x}_j^2}{p_j}\right) + o(N^{-L/2}), \quad (\text{S13})$$

where  $a_N$  is the reachable parity function in Equation (S1).

### 3. Level statistics of quantum density operators

This section outlines the framework for analyzing the spectral properties of the generated quantum thermal states. Level statistics, commonly applied to Hamiltonian energy spectra to diagnose quantum chaos and ergodicity [43, 46], extend naturally to density operators  $\rho$  via the modular Hamiltonian.

For a strictly positive density operator  $\rho$ , its spectral properties are closely related to those of the fictitious Hamiltonian governing the thermal distribution. We define the modular Hamiltonian  $H$  by  $\rho = \frac{e^{-H}}{\text{Tr}(e^{-H})}$ . The eigenvalues of  $\rho$ , denoted by  $\{p_i\}$ , are directly related to the spectrum of  $H$ , denoted by  $\{\xi_i\}$ , via the transformation  $\xi_i = -\ln(p_i) - \ln Z$ . The level statistics of  $\rho$  are thus analyzed through the unfolding of the "entanglement energies" or modular levels  $\{\xi_i\}$ .

To avoid the ambiguities associated with spectral unfolding in finite-size systems, we utilize the adjacent gap ratio statistics introduced by Oganesyan and Huse [43]. Let the sorted spectrum of the modular Hamiltonian be ordered such that  $\xi_1 \leq \xi_2 \leq \dots \leq \xi_D$ , where  $D$  is the dimension of the Hilbert space. We define the nearest-neighbor level spacing as:

$$\delta_n = \xi_{n+1} - \xi_n \geq 0. \quad (\text{S14})$$

The dimensionless level spacing ratio  $r_n$  is defined as:

$$r_n = \frac{\min(\delta_n, \delta_{n+1})}{\max(\delta_n, \delta_{n+1})} = \min\left(\tilde{r}_n, \frac{1}{\tilde{r}_n}\right) \in [0, 1] \quad (\text{S15})$$

where  $\tilde{r}_n = \delta_{n+1}/\delta_n$ . The distribution of  $r_n$ , denoted as  $P(r)$ , and its mean value  $\langle r \rangle$ , serve as robust indicators of the nature of the correlations in the quantum state. The following summarizes the known results of the average spacing ratios with respect to the specific RMT ensembles [58]:

- *Integrable (Poissonian) limit:* Systems with uncorrelated levels, typical of integrable models or localized phases, exhibit level spacings following a Poisson distribution with  $P(r) = \frac{2}{(1+r)^2}$  and  $\langle r \rangle_{\text{Poisson}} \approx 0.386$ .
- *Chaotic (Wigner–Dyson) limit:* Ergodic quantum systems exhibit level repulsion characteristic of Random Matrix Theory (RMT), with statistics depending on the symmetry class:  $\langle r \rangle_{\text{GOE}} \approx 0.536$  for systems with time-reversal symmetry, and  $\langle r \rangle_{\text{GUE}} \approx 0.603$  for systems without.

In our algorithm,  $\langle r \rangle$  values approaching the GUE/GOE limits in the sampled thermal states indicate that the generated state captures the complexity and correlations of a thermalizing many-body system. Conversely,  $\langle r \rangle \approx 0.39$  would suggest a failure to capture thermal correlations or an underlying integrability in the generator set.

### Appendix B: Thermal-drift channel

Let  $\sigma$  be an  $n$ -qubit Pauli operator and let  $\tau \in \mathbb{R}_+$ . We define the unnormalized imaginary-time evolution (ITE) maps at time  $\tau$  in the two opposite directions by

$$\mathcal{E}_\sigma^\uparrow(\rho) = e^{-\tau\sigma/2} \rho e^{-\tau\sigma/2} \quad \text{and} \quad \mathcal{E}_\sigma^\downarrow(\rho) = e^{+\tau\sigma/2} \rho e^{+\tau\sigma/2}. \quad (\text{S1})$$

Throughout this section, we use " $\uparrow\downarrow$ " to discuss both directions simultaneously. The goal is to construct a circuit that applies one of these two maps at random to an input state  $\rho$  on the main system and records the applied direction in an ancilla register.

To formalize this task, we introduce a  $2n$ -qubit ancilla system  $AB$  and the  $n$ -qubit main system  $S$ . Based on the identity that

$$\text{Tr}[\mathcal{E}_\sigma^\uparrow(\rho) + \mathcal{E}_\sigma^\downarrow(\rho)] = \text{Tr}[(e^{-\tau\sigma} + e^{\tau\sigma})\rho] = (e^\tau + e^{-\tau}) \text{Tr}[\rho] = 2 \cosh(\tau), \quad (\text{S2})$$

we define the thermal-drift channel  $\mathcal{N}_\sigma(\rho) : \mathcal{D}(\mathcal{H}_S) \rightarrow \mathcal{D}(\mathcal{H}_{ABS})$  satisfying

$$\text{Tr}_{AB}[\Pi_{AB}^{\uparrow\downarrow} \mathcal{N}_\sigma(\rho)] = \frac{1}{2 \cosh(\tau)} \mathcal{E}_\sigma^{\uparrow\downarrow}(\rho), \quad (\text{S3})$$

where  $\Pi^\pm$  are mutually orthogonal projectors on  $AB$  such that  $\Pi^\uparrow + \Pi^\downarrow \prec I_{AB}$ . Measuring the ancilla system  $AB$  in the projection-valued measure extending  $\{\Pi^\uparrow, \Pi^\downarrow\}$  reveals which branch of Equation (S3) occurred; the corresponding post-measurement state on  $S$  is obtained by tracing out  $AB$  and normalizing in the usual way.

The map satisfying Equation (S3) is completely positive and trace-preserving under the chosen normalization, and thus admits a unitary dilation. The next theorem provides an explicit implementation with  $\mathcal{O}(n)$  elementary gates, up to a heralded failure outcome  $\Pi^\circlearrowleft$ .

**Theorem S6** Suppose  $\tau > 0$  and  $\sigma$  is an  $n$ -qubit Pauli operator that has no local identity term. Then there exists a projection-valued measure  $\{\Pi^\uparrow, \Pi^\downarrow, \Pi^\circlearrowright\}$  on system  $AB$ , a  $\tau$ -dependent ansatz  $U_\tau$  and two fixed ansatzes  $T, V$ , such that the map  $\mathcal{N}_\approx : \mathcal{D}(\mathcal{H}_S) \rightarrow \mathcal{D}(\mathcal{H}_{ABS})$  constructed in Figure S1 (dashed area) satisfies for all  $\rho \in \mathcal{D}(\mathcal{H}_S)$ ,

$$\text{Tr}_{AB}[\Pi_{AB}^\circlearrowright \mathcal{N}_\approx(\rho)] = p\rho \quad \text{and} \quad \text{Tr}_{AB}[\Pi_{AB}^\uparrow \mathcal{N}_\approx(\rho)] = (1-p) \text{Tr}_{AB}[\Pi_{AB}^\uparrow \mathcal{N}_\sigma(\rho)], \quad (\text{S4})$$

where  $p^{-1} = 2 \cosh^2(\tau/2)$ ,  $\text{Tr}[\Pi^\uparrow] = \text{Tr}[\Pi^\downarrow]$  and  $\mathcal{N}_\sigma$  is given as in Equation (S3). Moreover, implementation of  $\mathcal{N}_\approx$  takes  $\mathcal{O}(n)$  single-qubit gates and CNOT gates; the projection-valued measure can be done in the computational basis.

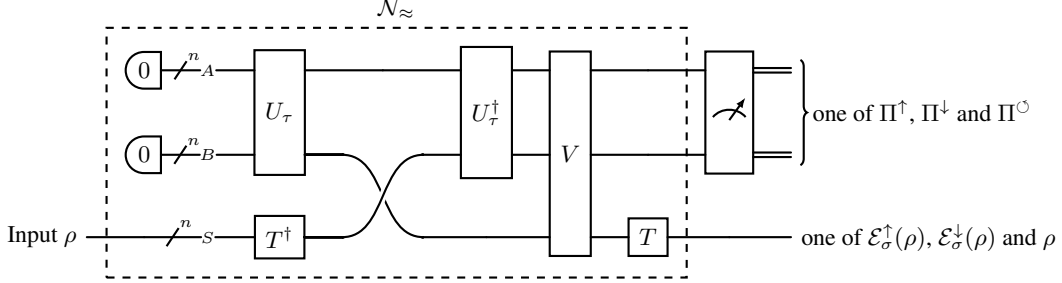


Fig S1. A circuit implementing the channel  $\mathcal{N}_\approx$ . Repeating  $\mathcal{N}_\approx$  and measuring  $AB$  in the computational basis until the outcome is not in  $\Pi^\circlearrowright$  implements  $\mathcal{N}_\sigma$ .

Theorem S6 assumes that the Pauli operator has no local identity term; the next theorem removes this restriction and provides the resource bound for implementing a random-direction Pauli ITE step.

**Theorem S7** Suppose  $\tau > 0$  and  $\sigma$  is an  $n$ -qubit Pauli operator. Then there exists a quantum channel  $\mathcal{N}_\sigma : \mathcal{D}(\mathcal{H}_S) \rightarrow \mathcal{D}(\mathcal{H}_{ABS})$  and a measure-and-trace operation  $\mathcal{M} : \mathcal{D}(\mathcal{H}_{ABS}) \rightarrow \{1, -1\} \times \mathcal{D}(\mathcal{H}_S)$  such that for all  $\rho \in \mathcal{D}(\mathcal{H}_S)$ ,

$$\mathcal{M} \circ \mathcal{N}_\sigma(\rho) = \begin{cases} (1, \mathcal{E}_\sigma^\uparrow(\rho) / \text{Tr}[e^{-\tau\sigma}\rho]), & \text{with probability } \text{Tr}[e^{-\tau\sigma}\rho] / (2 \cosh \tau); \\ (-1, \mathcal{E}_\sigma^\downarrow(\rho) / \text{Tr}[e^{\tau\sigma}\rho]), & \text{with probability } \text{Tr}[e^{\tau\sigma}\rho] / (2 \cosh \tau). \end{cases} \quad (\text{S5})$$

Moreover, one can use  $2n$  ancilla qubits and at most  $\mathcal{O}(n \log(1/\delta))$  single-qubit gates and CNOT gates to implement  $\mathcal{N}_\sigma$  with probability at least  $1 - \delta$ ;  $\mathcal{M}$  requires only computational-basis measurements and classical post-processing of the outcomes.

**Proof** We first consider the case where  $\sigma$  has no local identity term. Theorem S6 provides a projection-valued measure  $\{\Pi^\uparrow, \Pi^\downarrow, \Pi^\circlearrowright\}$  and a channel  $\mathcal{N}_\approx$  such that

$$\text{Tr}_{AB}[\Pi_{AB}^\circlearrowright \mathcal{N}_\approx(\rho)] = \frac{1}{2 \cosh^2(\tau/2)} \rho \quad \text{and} \quad \text{Tr}_{AB}[\Pi_{AB}^\uparrow \mathcal{N}_\approx(\rho)] = \left(1 - \frac{1}{2 \cosh^2(\tau/2)}\right) \text{Tr}_{AB}[\Pi_{AB}^\uparrow \mathcal{N}_\sigma(\rho)] \quad (\text{S6})$$

Measuring  $\mathcal{N}_\approx(\rho)$  on system  $AB$  with respect to  $\{\Pi^\circlearrowright, I_{AB} - \Pi^\circlearrowright\}$  partitions the output into a fallback branch to  $\rho$  and a success branch to  $\mathcal{N}_\sigma(\rho)$ . Define  $\mathcal{M}_\circlearrowright$  to be the operation that measures  $AB$  and, upon obtaining  $\Pi^\circlearrowright$ , traces out  $AB$  and outputs the remaining state on  $S$ ; define  $\mathcal{M}_{\uparrow\downarrow}$  analogously for the complementary event  $I_{AB} - \Pi^\circlearrowright$ . For an integer  $k \geq 1$ , consider the repeat-until-success map

$$\mathcal{M}_{\uparrow\downarrow} \circ \mathcal{N}_\approx + \mathcal{M}_{\uparrow\downarrow} \circ \mathcal{N}_\approx \circ \mathcal{M}_\circlearrowright \circ \mathcal{N}_\approx + \dots + \mathcal{M}_{\uparrow\downarrow} \circ \mathcal{N}_\approx \circ (\mathcal{M}_\circlearrowright \circ \mathcal{N}_\approx)^{\circ k}. \quad (\text{S7})$$

Since the fallback probability in each invocation is at most  $1/2$ , the probability of fallback in all  $k+1$  attempts is at most  $2^{-(k+1)}$ . Choosing  $k = \mathcal{O}(\log(1/\delta))$  ensures failure probability at most  $\delta$ . Each invocation of  $\mathcal{N}_\approx$  uses  $\mathcal{O}(n)$  elementary gates by Theorem S6, so the total gate count is  $\mathcal{O}(n \log(1/\delta))$ .

Conditioned on the success event  $I_{AB} - \Pi^\circlearrowright$ , the output is proportional to  $\mathcal{N}_\sigma(\rho)$  as defined in Equation (S3). We now define  $\mathcal{M}$  to measure  $AB$  with respect to  $\{\Pi^\uparrow, \Pi^\downarrow\}$ , trace out  $AB$ , and normalize the post-measurement state on  $S$ . Using  $\text{Tr}[\Pi^\uparrow] = \text{Tr}[\Pi^\downarrow] = 2^{2n-2}$  and the fact that  $\mathcal{E}_\sigma^\uparrow(\rho)$  and  $\mathcal{E}_\sigma^\downarrow(\rho)$  have traces  $\text{Tr}[e^{-\tau\sigma}\rho]$  and  $\text{Tr}[e^{\tau\sigma}\rho]$ , respectively, we obtain

$$\text{Pr}(m = 1) = \left(1 - \frac{1}{2 \cosh^2(\tau/2)}\right) \text{Tr}[\Pi_{AB}^\uparrow \mathcal{N}_\sigma(\rho)] = \frac{\text{Tr}[e^{-\tau\sigma}\rho]}{2 \cosh \tau}, \quad (\text{S8})$$

$$\Pr(m = -1) = \left(1 - \frac{1}{2 \cosh^2(\tau/2)}\right) \text{Tr}[\Pi_{AB}^\downarrow \mathcal{N}_\sigma(\rho)] = \frac{\text{Tr}[e^{\tau\sigma}\rho]}{2 \cosh \tau}. \quad (\text{S9})$$

Conditioning on each event yields the normalized post-measurement states  $\mathcal{E}_\sigma^\uparrow(\rho)/\text{Tr}[e^{-\tau\sigma}\rho]$  and  $\mathcal{E}_\sigma^\downarrow(\rho)/\text{Tr}[e^{\tau\sigma}\rho]$ , as stated.

We now extend the construction to a general  $\sigma$  that may contain local identity terms. Let  $\sigma'$  be the tensor product of the non-identity local Pauli terms of  $\sigma$ , and let  $P$  be an  $n$ -qubit permutation gate such that  $\sigma = P^\dagger(\sigma' \otimes I)P$ . For any  $\rho \in \mathcal{D}(\mathcal{H}_S)$ ,

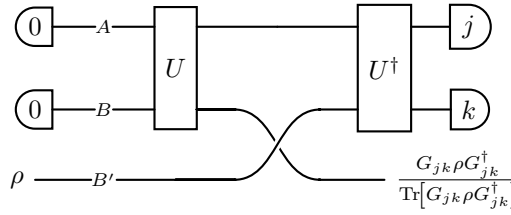
$$P^\dagger(\mathcal{E}_{\sigma'}^{\uparrow\downarrow} \otimes \mathbb{1})(P\rho P^\dagger)P = P^\dagger(e^{\mp\tau\sigma'/2} \otimes I)P \cdot \rho \cdot P^\dagger(e^{\mp\tau\sigma'/2} \otimes I)P \quad (\text{S10})$$

$$= e^{\mp\tau\sigma/2} \rho e^{\mp\tau\sigma/2} = \mathcal{E}_\sigma^{\uparrow\downarrow}(\rho). \quad (\text{S11})$$

Applying the above implementation to  $\sigma'$  (on the nontrivial subsystem) and conjugating by  $P$  therefore realizes the required instrument for  $\sigma$ . The permutation  $P$  can be implemented with at most  $\mathcal{O}(n)$  CNOT gates, so the overall gate complexity remains  $\mathcal{O}(n \log(1/\delta))$ .  $\blacksquare$

The remainder of this section proves Theorem S6 by explicitly constructing  $U_\tau$ ,  $T$ , and  $V$ . We start from a SWAP-based construction that realizes a family of Kraus operators from a unitary on a larger space.

**Lemma S8** *Suppose  $U$  is a unitary acting on a bipartite system  $AB$ . Then for  $G_{jk} = \text{Tr}_A[U|00\rangle\langle jk|U^\dagger]$  and an additional system  $B'$  such that  $|B'| = |B|$ , the following circuit of systems  $ABB'$  holds*



**Proof** Let  $U = \sum_{x,y,z,t} C_{xyzt}|xy\rangle\langle zt|$  and  $\text{SWAP} = \sum_{l,m}|lm\rangle\langle ml|$ . For the operator acting on  $B'$  conditioned on outcomes  $(j, k)$  on  $AB$ , we compute

$$(\langle j_A j_B | U^\dagger)_{AB} \text{SWAP}_{BB'} (U | k_A k_B \rangle)_{AB} \quad (\text{S12})$$

$$= \sum_{x,y,z,t,m,l} C_{j_A j_B zt}^* C_{xy k_A k_B} (\langle z|_A \otimes \langle t|_B) (|l\rangle\langle m|_B \otimes |m\rangle\langle l|_{B'}) (\langle x|_A \otimes \langle y|_B) \quad (\text{S13})$$

$$= \sum_{x,y,z,t,m,l} C_{j_A j_B zt}^* C_{xy k_A k_B} \delta_{z,x} \delta_{t,l} \delta_{m,y} |m\rangle\langle l|_{B'} \quad (\text{S14})$$

$$= \sum_{x,y,z,t} C_{j_A j_B zt}^* C_{xy k_A k_B} \delta_{z,x} |y\rangle\langle t| \quad (\text{S15})$$

$$= \text{Tr}_A \left[ \sum_{x,y,z,t} C_{j_A j_B zt}^* C_{xy k_A k_B} |xy\rangle\langle zt|_{AB} \right] = \text{Tr}_A [U | k_A k_B \rangle\langle j_A j_B | U^\dagger]. \quad (\text{S16})$$

For any pure state  $|\psi\rangle$  on  $B'$ , substituting this identity into the circuit shows that

$$U_{AB}^\dagger \text{SWAP}_{BB'} U_{AB} (|00\rangle \otimes |\psi\rangle) = \sum_{j,k} |jk\rangle\langle jk|_{AB} U_{AB}^\dagger \text{SWAP}_{BB'} U_{AB} (|00\rangle \otimes |\psi\rangle) \quad (\text{S17})$$

$$= \sum_{j,k} |jk\rangle_{AB} (\langle jk| U^\dagger)_{AB} \text{SWAP}_{BB'} (U |00\rangle)_{AB} |\psi\rangle_{B'} \quad (\text{S18})$$

$$= \sum_{j,k} |jk\rangle_{AB} G_{jk} |\psi\rangle_{B'} = \sum_{j,k} |jk\rangle \otimes G_{jk} |\psi\rangle. \quad (\text{S19})$$

When the system  $AB$  is measured to be  $jk$ , the unnormalized post-measurement state on  $B'$  is  $G_{jk}|\psi\rangle$ , and hence the normalized post-measurement state is  $G_{jk}|\psi\rangle/\|G_{jk}|\psi\rangle\|$ . By linearity, the same conclusion holds for a mixed input  $\rho$ , yielding the claimed output state  $G_{jk}\rho G_{jk}^\dagger / \text{Tr}[G_{jk}\rho G_{jk}^\dagger]$ .  $\blacksquare$

We now prove Theorem S6. All three systems  $A, B, S$  are  $n$ -qubit. In the following analysis,  $A_i$  denotes the  $i$ -th qubit in system  $A$  (counting from top to bottom), and similarly for  $B$  and  $S$ .

**Theorem S6 (Detailed version)** Suppose  $\tau > 0$  and  $\sigma$  is an  $n$ -qubit Pauli operator that has no local identity term. Consider the following construction of a projection-valued measure on the system  $AB$ ,

$$\Pi^\circlearrowleft = |1\rangle\langle 1|_{A_n}, \quad \Pi^\uparrow = |0\rangle\langle 0|_{A_n} \otimes |0\rangle\langle 0|_{B_n}, \quad \Pi^\downarrow = |0\rangle\langle 0|_{A_n} \otimes |1\rangle\langle 1|_{B_n}, \quad (\text{S20})$$

and of circuit ansatzes on system  $ABS$ ,

$$U_\tau = \left( \prod_{i=1}^n \text{CNOT}_{A_i B_i} \right) \left( \prod_{i=1}^{n-1} \text{CNOT}_{A_i A_n} \right) \left( H^{\otimes(n-1)} \otimes R_y(2\theta) \right)_A, \quad (\text{S21})$$

$$V = \left( \prod_{i=1}^n \text{CNOT}_{B_i B_n} \right) \left( \prod_{i=1}^n \text{CNOT}_{B_i S_i} \text{CZ}_{A_i S_i} \right) \left( \prod_{i=1}^{n-1} \text{CNOT}_{A_n A_i} \right), \quad (\text{S22})$$

$$T \text{ satisfies } TZ^{\otimes n} T^\dagger = \sigma, \quad (\text{S23})$$

where  $\theta = \arccos \sqrt{e^{-\tau/2}/(2 \cosh(\tau/2))}$ . Then the map  $\mathcal{N}_\approx$  constructed in Figure S1 (dashed area) satisfies

$$\text{Tr}_{AB} [\Pi_{AB}^\circlearrowleft \mathcal{N}_\approx(\rho)] = \frac{1}{2 \cosh^2(\tau/2)} \rho \quad \text{and} \quad \text{Tr}_{AB} [\Pi_{AB}^{\uparrow\downarrow} \mathcal{N}_\approx(\rho)] = \frac{1}{4 \cosh^2(\tau/2)} \mathcal{E}_\sigma^{\uparrow\downarrow}(\rho). \quad (\text{S24})$$

**Proof** The proof is decomposed into two parts: we first (1) analyze what  $G_{jk}$  is by taking  $U_\tau$  into Lemma S8, and show that (2)  $V$  can decode, map and group these  $G_{jk}$  to be either  $e^{-\tau\sigma/2}$ ,  $e^{\tau\sigma/2}$  or the identity matrix. Taking the whole picture gives the statement.

(1) For the first part, one can derive that for all  $|j\rangle = |j_1 \cdots j_n\rangle$  in system  $A$ ,

$$\left( \prod_{i=1}^{n-1} \text{CNOT}_{A_i A_n} \right) \left( H^{\otimes(n-1)} \otimes R_y(2\theta) \right) |j\rangle \quad (\text{S25})$$

$$= \left( \prod_{i=1}^{n-1} \text{CNOT}_{A_i A_n} \right) \left( H^{\otimes(n-1)} |j_{1:n}\rangle \otimes R_y(2\theta) |j_n\rangle \right) \quad (\text{S26})$$

$$= \frac{1}{\sqrt{2^{n-1}}} \left( \prod_{i=1}^{n-1} \text{CNOT}_{A_i A_n} \right) \sum_{x \in \{0,1\}^{n-1}} (-1)^{x \cdot j_{1:n}} |x\rangle \otimes (\cos(\theta) |j_n\rangle + (-1)^{j_n} \sin(\theta) X |j_n\rangle) \quad (\text{S27})$$

$$= \frac{1}{\sqrt{2^{n-1}}} \sum_{x \in \{0,1\}^{n-1}} (-1)^{x \cdot j_{1:n}} |x\rangle \otimes \left( \cos(\theta) |j_n \oplus p(x)\rangle + (-1)^{j_n} \sin(\theta) |j_n \oplus p(x) \oplus 1\rangle \right), \quad (\text{S28})$$

where  $j_{1:n} = j_1 \cdots j_{n-1}$ ,  $\oplus$  is the bitwise addition and  $p(x)$  is the bitwise parity function defined in Equation (S2). Taking the last piece of  $U_\tau$  gives

$$U_\tau |jk\rangle = \left( \prod_{i=1}^n \text{CNOT}_{A_i B_i} \right) \left( \prod_{i=1}^{n-1} \text{CNOT}_{A_i A_n} \right) \left( H^{\otimes(n-1)} \otimes R_y(2\theta) \right) (|j\rangle_A \otimes |k\rangle_B) \quad (\text{S29})$$

$$= \left( \prod_{i=1}^n \text{CNOT}_{A_i B_i} \right) \frac{1}{\sqrt{2^{n-1}}} \sum_{x \in \{0,1\}^{n-1}} (-1)^{x \cdot j_{1:n}} |x\rangle_{A_{1:n}} \otimes \left( \cos(\theta) |j'_n\rangle_{A_n} + (-1)^{j_n} \sin(\theta) |j'_n \oplus 1\rangle_{A_n} \right) \otimes |k\rangle_B \quad (\text{S30})$$

$$= \sum_{x \in \{0,1\}^{n-1}} \frac{(-1)^{x \cdot j_{1:n}}}{\sqrt{2^{n-1}}} |x\rangle_{A_{1:n}} |k_{1:n} \oplus x\rangle_{B_{1:n}} \left( \cos(\theta) |j'_n\rangle_{A_n} |k'_n\rangle_{B_n} + (-1)^{j_n} \sin(\theta) |j'_n \oplus 1\rangle_{A_n} |k'_n \oplus 1\rangle_{B_n} \right) \quad (\text{S31})$$

for  $j'_n = j_n \oplus p(x)$  and  $k'_n = k_n \oplus j'_n$ . When  $j$  and  $k$  are both zero, we have

$$U_\tau |00\rangle = \frac{1}{\sqrt{2^{n-1}}} \sum_{x \in \{0,1\}^{n-1}} |x\rangle_{A_{1:n}} |x\rangle_{B_{1:n}} \left( \cos(\theta) |p(x)\rangle_{A_n} |p(x)\rangle_{B_n} + \sin(\theta) |p(x) \oplus 1\rangle_{A_n} |p(x) \oplus 1\rangle_{B_n} \right). \quad (\text{S32})$$

Then we have

$$U_\tau |00\rangle\langle jk| U_\tau^\dagger = \frac{1}{2^{n-1}} \sum_{x \in \{0,1\}^{n-1}} (-1)^{x \cdot j_{1:n}} |x\rangle\langle x|_{A_{1:n}} |x\rangle\langle k_{1:n} \oplus x|_{B_{1:n}}. \quad (\text{S33})$$

$$\left( \cos(\theta)|p(x)\rangle_{A_n}|p(x)\rangle_{B_n} + \sin(\theta)|p(x) \oplus 1\rangle_{A_n}|p(x) \oplus 1\rangle_{B_n} \right). \quad (\text{S34})$$

$$\left( \cos(\theta)\langle j'_n|_{A_n}\langle k'_n|_{B_n} + (-1)^{j_n} \sin(\theta)\langle j'_n \oplus 1|_{A_n}\langle k'_n \oplus 1|_{B_n} \right). \quad (\text{S35})$$

$G_{jk}$  in Lemma S8 is given as

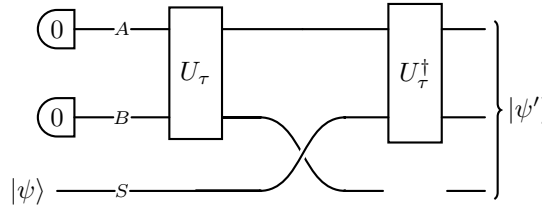
$$G_{jk} = \text{Tr}_A[U_\tau|00\rangle\langle jk|U_\tau^\dagger] = \frac{1}{2^{n-1}} \sum_{x \in \{0,1\}^{n-1}} (-1)^{x \cdot j_{1:n}} |x\rangle\langle k_{1:n} \oplus x| \otimes Q_{j_n k_n}, \quad (\text{S36})$$

where  $Q_{j_n k_n}$  is constructed as

$$Q_{j_n k_n} = \delta_{p(x), j'_n} (\cos^2(\theta)|p(x)\rangle\langle k'_n| + (-1)^{j_n} \sin^2(\theta)X|p(x)\rangle\langle k'_n|X) + \quad (\text{S37})$$

$$\frac{1}{2}\delta_{p(x), (j'_n \oplus 1)} \sin(2\theta) (X|p(x)\rangle\langle k'_n| + (-1)^{j_n}|p(x)\rangle\langle k'_n|X). \quad (\text{S38})$$

(2) For the second part, without loss of generality, suppose  $\rho = |\psi\rangle\langle\psi|$  is a pure state. At this point, by Lemma S8, the output state  $|\psi'\rangle$  of the following circuit



can be expressed as  $|\psi'\rangle = \sum_{j,k} |jk\rangle \otimes G_{jk}|\psi\rangle$ . Then

$$V|\psi'\rangle = \left( \prod_{i=1}^n \text{CNOT}_{B_i B_n} \right) \left( \prod_{i=1}^n \text{CNOT}_{B_i S_i} \text{CZ}_{A_i S_i} \right) \left( \prod_{i=1}^{n-1} \text{CNOT}_{A_n A_i} \right) \sum_{j,k} |j\rangle \otimes |k\rangle \otimes G_{jk}|\psi\rangle \quad (\text{S39})$$

$$= \left( \prod_{i=1}^n \text{CNOT}_{B_i B_n} \right) \left( \prod_{i=1}^n \text{CNOT}_{B_i S_i} \text{CZ}_{A_i S_i} \right) \sum_{j,k} \left( \bigotimes_{i=1}^{n-1} |j_i \oplus j_n\rangle \right) \otimes |j_n\rangle \otimes |k\rangle \otimes G_{jk}|\psi\rangle \quad (\text{S40})$$

$$= \left( \prod_{i=1}^n \text{CNOT}_{B_i B_n} \right) \left( \prod_{i=1}^n \text{CNOT}_{B_i S_i} \right) \left( \prod_{i=1}^n \text{CZ}_{A_i S_i} \right) \sum_{j,k} \left( \bigotimes_{i=1}^{n-1} |j_i \oplus j_n\rangle \right) \otimes |j_n\rangle \otimes |k\rangle \otimes G_{jk}|\psi\rangle \quad (\text{S41})$$

$$= \left( \prod_{i=1}^n \text{CNOT}_{B_i B_n} \right) \sum_{j,k} \left( \bigotimes_{i=1}^{n-1} |j_i \oplus j_n\rangle \right) \otimes |j_n\rangle \otimes |k\rangle \otimes E_{jk}|\psi\rangle \quad (\text{S42})$$

$$= \sum_{j,k} \left( \bigotimes_{i=1}^{n-1} |j_i \oplus j_n\rangle \right) \otimes |j_n\rangle \otimes |k_{1:n}\rangle \otimes |p(k)\rangle \otimes E_{jk}|\psi\rangle \quad (\text{S43})$$

for  $E_{jk}$  constructed as

$$E_{jk} = X^{(k)} \left( \prod_{i=1}^{n-1} Z_{S_i}^{j_i + j_n} \right) Z_{S_n}^{j_n} G_{jk}, \quad (\text{S44})$$

where  $X^{(k)}$  is short for  $\bigotimes_{i=1}^n X^{k_i}$ . Now we analyze what  $E_{jk}$  will be for three cases:  $j_n = 1$ ,  $(j_n, p(k)) = (0, 0)$  and  $(j_n, p(k)) = (0, 1)$ .

If  $j_n = 1$ , then  $j'_n = j_n \oplus p(x) = p(x) \oplus 1$ ,  $k'_n = k_n \oplus j'_n = k_n \oplus p(x) \oplus 1$  and  $Q_{j_n k_n}$  in Equation (S37) satisfies

$$Q_{j_n k_n} = \frac{1}{2} \sin(2\theta) (X|p(x)\rangle\langle k_n \oplus p(x)|X - |p(x)\rangle\langle k_n \oplus p(x)|) \quad (\text{S45})$$

and hence

$$G_{jk} = \frac{1}{2^n} \sin(2\theta) \sum_{x \in \{0,1\}^{n-1}} (-1)^{x \cdot j_{1:n}} |x\rangle\langle k_{1:n} \oplus x| \otimes (X|p(x)\rangle\langle k_n \oplus p(x)|X - |p(x)\rangle\langle k_n \oplus p(x)|) \quad (\text{S46})$$

and hence

$$E_{jk} = \frac{\sin(2\theta)}{2^n} X^{(k)} \left( \prod_{i=1}^{n-1} Z_{S_i}^{j_i+1} \right) Z_{S_n} \sum_{x \in \{0,1\}^{n-1}} (-1)^{x \cdot j_{1:n}} |x\rangle \langle k_{1:n} \oplus x| \otimes (X|p(x)\rangle \langle k_n \oplus p(x)|X - |p(x)\rangle \langle k_n \oplus p(x)|) \quad (\text{S47})$$

$$= \frac{\sin(2\theta)}{2^n} X^{(k)} \sum_{x \in \{0,1\}^{n-1}} (-1)^x |x\rangle \langle k_{1:n} \oplus x| \otimes \left( (-1)^{p(x)+1} |p(x) \oplus 1\rangle \langle k_n \oplus p(x) \oplus 1| - (-1)^{p(x)} |p(x)\rangle \langle k_n \oplus p(x)| \right) \quad (\text{S48})$$

$$= \frac{\sin(2\theta)}{2^n} \sum_{x \in \{0,1\}^{n-1}} (-1)^x |x \oplus k_{1:n}\rangle \langle k_{1:n} \oplus x| \otimes (-1)^{p(x)+1} (|p(x) \oplus k_n \oplus 1\rangle \langle k_n \oplus p(x) \oplus 1| + |p(x) \oplus k_n\rangle \langle k_n \oplus p(x)|) \quad (\text{S49})$$

$$= -\frac{\sin(2\theta)}{2^n} \sum_{x \in \{0,1\}^{n-1}} |x \oplus k_{1:n}\rangle \langle k_{1:n} \oplus x| \otimes I = -\frac{1}{2^n} \sin(2\theta) I_S. \quad (\text{S50})$$

If  $j_n = 0$ , then  $j'_n = j_n \oplus p(x) = p(x)$ ,  $k'_n = k_n \oplus j'_n = k_n \oplus p(x)$  and hence

$$Q_{j_n k_n} = \cos^2(\theta) |p(x)\rangle \langle k_n \oplus p(x)| + \sin^2(\theta) X|p(x)\rangle \langle k_n \oplus p(x)|X \quad (\text{S51})$$

$$\implies G_{jk} = \frac{1}{2^{n-1}} \sum_{x \in \{0,1\}^{n-1}} (-1)^{x \cdot j_{1:n}} |x\rangle \langle k_{1:n} \oplus x| \otimes (\cos^2(\theta) |p(x)\rangle \langle k_n \oplus p(x)| + \sin^2(\theta) X|p(x)\rangle \langle k_n \oplus p(x)|X), \quad (\text{S52})$$

and hence

$$E_{jk} = X^{(k)} Z_{S_{1:n}}^{(j_{1:n})} G_{jk} \quad (\text{S53})$$

$$= \frac{1}{2^{n-1}} X^{(k)} \sum_{x \in \{0,1\}^{n-1}} |x\rangle \langle k_{1:n} \oplus x| \otimes (\cos^2(\theta) |p(x)\rangle \langle k_n \oplus p(x)| + \sin^2(\theta) X|p(x)\rangle \langle k_n \oplus p(x)|X) \quad (\text{S54})$$

$$= \frac{1}{2^{n-1}} X^{(k)} \left[ \sum_{x \in \{0,1\}^{n-1}} |x\rangle \langle x| \otimes (\cos^2(\theta) |p(x)\rangle \langle p(x)| + \sin^2(\theta) X|p(x)\rangle \langle p(x)|X) \right] X^{(k)}. \quad (\text{S55})$$

Denote  $C = 2 \cosh(\tau/2) = e^{-\tau/2} + e^{\tau/2}$ . Since  $\cos^2(\theta) = e^{-\tau/2}/C$  and  $\sin^2(\theta) = e^{\tau/2}/C$ , the expression surrounded by the square bracket is simplified as

$$\sum_{x \in \{0,1\}^{n-1}} |x\rangle \langle x| \otimes (\cos^2(\theta) |p(x)\rangle \langle p(x)| + \sin^2(\theta) X|p(x)\rangle \langle p(x)|X) \quad (\text{S56})$$

$$= \frac{1}{C} \sum_{x \in \{0,1\}^{n-1}} |x\rangle \langle x| \otimes \left( e^{-\tau/2} |p(x)\rangle \langle p(x)| + e^{\tau/2} |p(x) \oplus 1\rangle \langle p(x) \oplus 1| \right) \quad (\text{S57})$$

$$= \frac{1}{C} \sum_{x \in \{0,1\}^{n-1}} |x\rangle \langle x| \otimes \exp\left(-\frac{\tau}{2}(-1)^{p(x)} Z\right) = \frac{1}{C} e^{-\tau Z^{\otimes n}/2}, \quad (\text{S58})$$

where the last equality comes from the fact that  $Z^{\otimes(n-1)}|x\rangle = (-1)^{p(x)}|x\rangle$ . Then

$$E_{jk} = \frac{1}{2^{n-1}C} X^{(k)} e^{-\tau Z^{\otimes n}/2} X^{(k)} \quad (\text{S59})$$

$$= \frac{1}{2^{n-1}C} \begin{cases} e^{-\tau Z^{\otimes n}/2}, & \text{if } p(k) = 0, \\ e^{\tau Z^{\otimes n}/2}, & \text{if } p(k) = 1. \end{cases} \quad (\text{S60})$$

As a result, omitting subsystems  $A_{1:n}$  and  $B_{1:n}$ , since  $TZ^{\otimes n}T^\dagger = \sigma$ , we have

$$T_S V T_S^\dagger |\psi'\rangle = \sum_{j,k} \dots \otimes |j_n\rangle_{A_n} \otimes |p(k)\rangle_{B_n} \otimes T E_{jk} T^\dagger |\psi\rangle \quad (\text{S61})$$

$$= - \sum_{j_n=1} \dots \otimes |1\rangle_{A_n} \otimes |p(k)\rangle_{B_n} \otimes \frac{1}{2^n} \sin(2\theta) |\psi\rangle + \quad (\text{S62})$$

$$+ \sum_{(j_n, p(k))=(0,0)} \dots \otimes |0\rangle_{A_n} \otimes |0\rangle_{B_n} \otimes \frac{1}{2^{n-1}C} e^{-\tau\sigma/2} |\psi\rangle + \quad (\text{S63})$$

$$+ \sum_{(j_n, p(k))=(0,1)} \dots \otimes |0\rangle_{A_n} \otimes |1\rangle_{B_n} \otimes \frac{1}{2^{n-1}C} e^{\tau\sigma/2} |\psi\rangle. \quad (\text{S64})$$

There are  $2^{2n-1}$ ,  $2^{2n-2}$ ,  $2^{2n-2}$  pairs of  $(j, k)$  for satisfying  $j_n = 1$ ,  $(j_n, p(k)) = (0, 0)$  and  $(j_n, p(k)) = (0, 1)$ , respectively. Finally, taking  $\Pi_{AB}^\circlearrowleft$ ,  $\Pi_{AB}^\uparrow$ ,  $\Pi_{AB}^\downarrow$  in Equation (S20) gives

$$\text{Tr}_{AB} [\Pi_{AB}^\circlearrowleft \mathcal{N}_{\approx} (|\psi\rangle\langle\psi|)] = 2^{2n-1} \cdot \frac{1}{2^{2n}} \sin^2(2\theta) |\psi\rangle\langle\psi| = \frac{1}{2 \cosh^2(\tau/2)} |\psi\rangle\langle\psi|, \quad (\text{S65})$$

$$\text{Tr}_{AB} [\Pi_{AB}^\uparrow \mathcal{N}_{\approx} (|\psi\rangle\langle\psi|)] = 2^{2n-2} \cdot \frac{1}{2^{2n-2}C^2} e^{-\tau\sigma/2} |\psi\rangle\langle\psi| e^{-\tau\sigma/2} = \frac{1}{4 \cosh^2(\tau/2)} \mathcal{E}_\sigma^\uparrow (|\psi\rangle\langle\psi|), \quad (\text{S66})$$

$$\text{Tr}_{AB} [\Pi_{AB}^\downarrow \mathcal{N}_{\approx} (|\psi\rangle\langle\psi|)] = 2^{2n-2} \cdot \frac{1}{2^{2n-2}C^2} e^{\tau\sigma/2} |\psi\rangle\langle\psi| e^{\tau\sigma/2} = \frac{1}{4 \cosh^2(\tau/2)} \mathcal{E}_\sigma^\downarrow (|\psi\rangle\langle\psi|). \quad (\text{S67})$$

The statement holds by generalizing  $|\psi\rangle\langle\psi|$  to  $\rho$  by linearity.  $\blacksquare$

### Appendix C: Sampling thermal states and their labels

Let  $\beta > 0$  and let  $\Sigma = \{\sigma_j\}_{j=1}^L$  be a set of  $L$   $n$ -qubit Pauli operators with a boundary vector  $h \in \mathbb{R}_+^L$ . The goal of thermal state sampling is to sample a datum  $(H, G_{\beta, H})$  from the dataset

$$S(\beta, \Sigma, h) = \left\{ (H, G_{\beta, H}) : H = \sum_{j=1}^L c_j \sigma_j, |c_j| \leq h_j, c_j \in \mathbb{R}, \sigma_j \in \Sigma \right\} \quad (\text{S1})$$

where  $G_{\beta, H} = e^{-\beta H} / \text{Tr}[e^{-\beta H}]$  is the thermal state of the Hamiltonian  $H$  at temperature  $\beta^{-1}$ . To avoid sampling continuous coefficients directly, we sample from a quantized surrogate. For  $N \geq 1$  define

$$S_N(\beta, \Sigma, h) = \left\{ (H, G_{\beta, H}) : H = \sum_{j=1}^L c_j \sigma_j, |c_j| \leq h_j, c_j/h_j \in (1/N)\mathbb{Z}, \sigma_j \in \Sigma \right\} \quad (\text{S2})$$

so that  $\bigcup_{N \geq 1} S_N(\beta, \Sigma, h)$  is dense in  $S(\beta, \Sigma, h)$  with respect to the sup-norm on the coefficient vector. The following algorithm describes how to sample a data from  $S_N(\beta, \Sigma, h)$ .

---

#### Algorithm 1: Pseudo code for our thermal state sampler

---

**Input** : Inverse temperature  $\beta$ , a set  $\Sigma$  of  $n$ -qubit Pauli operators with a boundary vector  $h$ , a number of steps  $N$ , a classical function SAMPLE that returns an value  $j$  with weight  $p_j = h_j/\lambda$ .

**Output**: A datum  $(H, G_{\beta, H}) \in S_N(\beta, \Sigma, h)$

- 1  $\tau \leftarrow \lambda\beta/N$ ;
- 2  $\rho \leftarrow I^{\otimes n}/2^n$ ;
- 3 **for**  $k = 1, \dots, N$  **do**
- 4     $j_k \leftarrow \text{SAMPLE}();$
- 5     $\mathcal{M}_{j_k}, \mathcal{N}_{\sigma_{j_k}} \leftarrow \text{Theorem S7 wrt. } \sigma_{j_k}.$
- 6     $(m_k, \rho) \leftarrow (\mathcal{M}_{j_k} \circ \mathcal{N}_{\sigma_{j_k}})(\rho);$
- 7     $c_j \leftarrow \lambda \sum_{k: j_k=j} m_k/N, H \leftarrow \sum_{j=1}^L c_j \sigma_j;$
- 8 **return**  $(H, \rho)$

---

This section develops two technical components used to analyze Algorithm 1. First, we prove the trace-norm error bound between the algorithmic output state and the target thermal state (Theorem 1). Second, we set up the random-walk viewpoint for the induced Hamiltonian coefficients, which underlies the sampling-probability analysis in Theorem 2.

### 1. Error analysis

Fix the step number  $N$  and a sequence of indices  $(j_k)_{k=1}^N \subset [L]$  selecting Pauli operators from  $\Sigma = \{\sigma_j\}_{j=1}^L$ , as in Algorithm 1. Let  $\rho_k$  denote the (normalized) system state after  $k$  steps, and define the step size  $\tau = \lambda\beta/N$ . Then  $(\rho_k)_{k=0}^N$  evolves according to the Markovian update rule

$$\rho_0 = I/2^n, \quad \rho_k = \mathcal{M}_{j_k} \circ \mathcal{N}_{j_k}(\rho_{k-1}) = \frac{e^{B_k} \rho_{k-1} e^{B_k}}{\text{Tr}[e^{B_k} \rho_{k-1} e^{B_k}]}, \quad (\text{S3})$$

where  $\mathcal{M}_{j_k}, \mathcal{N}_{j_k}$  are specified by Theorem S7 for  $\sigma_{j_k}$ . The corresponding random variable  $B_k$  takes the form

$$B_k = \begin{cases} \tau\sigma_{j_k}/2, & \text{with probability } \text{Tr}[e^{\tau\sigma_{j_k}} \rho_{k-1}]/2 \cosh \tau, \\ -\tau\sigma_{j_k}/2, & \text{with probability } \text{Tr}[e^{-\tau\sigma_{j_k}} \rho_{k-1}]/2 \cosh \tau. \end{cases} \quad (\text{S4})$$

Iterating Equation (S3) shows that the final output state can be written as

$$\rho_N = \frac{(\prod_{k=N}^1 e^{B_k}) \rho_0 (\prod_{k=1}^N e^{B_k})}{\text{Tr}[\text{ same above}]} = \frac{(\prod_{k=N}^2 e^{B_k}) e^{2B_1} (\prod_{k=2}^N e^{B_k})}{\text{Tr}[\text{ same above}]}, \quad (\text{S5})$$

where  $\prod_{k=N}^2$  denotes the ordered product from  $N$  down to 2. The corresponding target thermal state is

$$G_{\beta, H} = \frac{e^{-\beta H}}{\text{Tr}[e^{-\beta H}]} \quad \text{for} \quad H = -\frac{2}{\beta} \sum_{k=1}^N B_k. \quad (\text{S6})$$

In this subsection, we prove Theorem 1, which shows that, with probability at least  $1 - \delta$  and for sufficiently large  $N$ ,

$$\|\rho_N - G_{\beta, H}\|_1 \leq \mathcal{O}\left((n + \log(N/\delta))^{3/2} \lambda^3 \beta^3 N^{-3/2}\right). \quad (\text{S7})$$

Two lemmas simplify the proof. The first lemma compares the palindromic product in  $\rho_N$  with the exponential of the accumulated generator.

**Lemma S10** *Let  $(B_k)_{k=1}^N$  be a sequence of matrices. Denote  $S_k = \sum_{j=1}^k B_j$ . Suppose  $\max_{1 \leq j \leq N} \|B_j\|_\infty = \tau \ll 1$ . Then*

$$\log \left( \left( \prod_{j=N}^2 e^{B_j} \right) e^{2B_1} \left( \prod_{j=2}^N e^{B_j} \right) \right) = 2S_N + \Delta_N + \mathcal{R}_N, \quad (\text{S8})$$

where  $\Delta_k = -\frac{1}{6} \sum_{j=2}^k [B_j + 2S_{j-1}, [B_j, 2S_{j-1}]]$  denotes the terms of order 3 and  $\mathcal{R}_N$  denotes the remainder terms. We have

$$\|\mathcal{R}_N\|_\infty = \mathcal{O}\left(\sum_{r=5, r \text{ is odd}}^{\infty} \frac{1}{r!} \sum_{k=2}^N \|\text{ad}_{2S_{k-1}}^{r-1}(B_k)\|_\infty\right). \quad (\text{S9})$$

**Proof** For Hermitian  $X$  and  $Y$ , since  $(e^X e^Y e^X)^{-1} = e^{-X} e^{-Y} e^{-X}$ , we have

$$\log(e^X e^Y e^X) + \log(e^{-X} e^{-Y} e^{-X}) = 0, \quad (\text{S10})$$

which implies  $f(X, Y) = \log(e^X e^Y e^X) = -f(-X, -Y)$ . Hence, the BCH expansion of  $\log(e^X e^Y e^X)$  contains no even-order terms.

We proceed by induction using the palindromic products

$$M_k := \left( \prod_{j=k}^2 e^{B_j} \right) e^{2B_1} \left( \prod_{j=2}^k e^{B_j} \right), \quad Z_k := \log(M_k). \quad (\text{S11})$$

We have  $M_1 = e^{2B_1}$ , and for  $k \geq 2$ ,  $M_k = e^{B_k} M_{k-1} e^{B_k} = e^{B_k} e^{Z_{k-1}} e^{B_k}$ .

For  $k = 1$ , we have  $Z_1 = \log(e^{2B_1}) = 2B_1 = 2S_1$ , so the claim holds.

Now fix  $k \geq 2$  and assume inductively that  $Z_{k-1} = 2S_{k-1} + \Delta_{k-1} + \mathcal{R}_{k-1}$ , where  $\Delta_{k-1}$  collects the cubic terms and  $\mathcal{R}_{k-1}$  collects the remaining odd-order terms of degree at least 5. Applying Lemma S3 to  $e^{B_k} e^{Z_{k-1}} e^{B_k}$  gives

$$Z_k = \log(e^{B_k} e^{Z_{k-1}} e^{B_k}) \quad (\text{S12})$$

$$= \log(e^{B_k} e^{2S_{k-1} + \Delta_{k-1} + \mathcal{R}_{k-1}} e^{B_k}) \quad (\text{S13})$$

$$= 2S_k + \Delta_{k-1} + \mathcal{R}_{k-1} - \frac{1}{6} [B_k + 2S_{k-1} + \Delta_{k-1} + \mathcal{R}_{k-1}, [B_k, 2S_{k-1} + \Delta_{k-1} + \mathcal{R}_{k-1}]]. \quad (\text{S14})$$

Separating the cubic contribution from higher-order terms yields

$$\Delta_k = \Delta_{k-1} - \frac{1}{6} [B_k + 2S_{k-1}, [B_k, 2S_{k-1}]], \quad (\text{S15})$$

$$\mathcal{R}_k = \mathcal{R}_{k-1} - \frac{1}{6} [B_k + 2S_{k-1}, [B_k, \Delta_{k-1} + \mathcal{R}_{k-1}]] - \frac{1}{6} [\Delta_{k-1} + \mathcal{R}_{k-1}, [B_k, 2S_{k-1} + \Delta_{k-1} + \mathcal{R}_{k-1}]]. \quad (\text{S16})$$

Iterating the recursion for  $\Delta_k$  gives

$$\Delta_N = \Delta_{N-1} - \frac{1}{6} [B_N + 2S_{N-1}, [B_N, 2S_{N-1}]] \quad (\text{S17})$$

$$= -\frac{1}{6} \sum_{k=2}^N [B_k + 2S_{k-1}, [B_k, 2S_{k-1}]]. \quad (\text{S18})$$

It remains to bound the remainder terms in  $\mathcal{R}_N$ . Write  $\mathcal{R}_k = \sum_{r \geq 5, r \text{ odd}} \mathcal{R}_{k,r}$ , where  $\mathcal{R}_{k,r}$  denotes the homogeneous terms of total order  $r$ , and assume  $\|B_k\|_\infty = \mathcal{O}(\|S_{k-1}\|_\infty)$  for  $k \geq 2$ . From the recursive definition of  $\mathcal{R}_k$ , the order- $r$  component obeys

$$\mathcal{R}_{k,r} = \mathcal{R}_{k-1,r} + \frac{1}{6} [B_k + 2S_{k-1}, [\mathcal{R}_{k-1,r-2}, B_k]] + \frac{1}{6} \sum_{j=3}^{r-4} [\mathcal{R}_{k-1,j}, [\mathcal{R}_{k-1,r-1-j}, B_k]]. \quad (\text{S19})$$

We claim that, for each odd  $r \geq 5$ , the increment  $\mathcal{R}_{k,r} - \mathcal{R}_{k-1,r}$  is dominated (up to constants depending only on  $r$ ) by terms of the form  $\text{ad}_{2S_{k-1}}^{r-1}(B_k)$ . The claim is immediate for  $r = 5$ , and the recursion preserves the dominance for higher odd orders.

Finally, since the coefficient of  $\text{ad}_X^{r-1}(Y)$  in the BCH expansion of  $\log(e^X e^Y e^X)$  has magnitude  $2/r!$ , there exists a constant  $C_r$  (depending only on  $r$ ) such that, for all odd  $r \geq 5$ ,

$$\|\mathcal{R}_{N,r}\|_\infty \leq \frac{C_r}{r!} \sum_{k=2}^N \|\text{ad}_{2S_{k-1}}^{r-1}(B_k)\|_\infty. \quad (\text{S20})$$

Summing over odd  $r \geq 5$  gives the stated bound on  $\|\mathcal{R}_N\|_\infty$ . ■

The second lemma controls the effect of normalizing matrix exponentials.

**Lemma S11** *Let  $A, E$  be two Hermitian matrices. Then*

$$\left\| \frac{e^{A+E}}{\text{Tr}[e^{A+E}]} - \frac{e^A}{\text{Tr}[e^A]} \right\|_1 \leq 2\|E\|_\infty. \quad (\text{S21})$$

**Proof** Consider  $t \in [0, 1]$ ,  $A(t) = A + tE$  and  $\rho(t) = e^{A(t)}/\mathcal{Z}(t)$  with  $\mathcal{Z}(t) = \text{Tr}[e^{A(t)}]$ . By Lemma S1, we have

$$\frac{d}{dt} e^{A(t)} = \int_0^1 e^{sA(t)} E e^{(1-s)A(t)} ds. \quad (\text{S22})$$

Differentiating  $\rho(t) = e^{A(t)}/\mathcal{Z}(t)$  gives

$$\frac{d}{dt} \rho(t) = \frac{d}{dt} \left( e^{A(t)} \cdot \frac{1}{\mathcal{Z}(t)} \right) = F(t) - \rho(t) \text{Tr}[F(t)], \quad (\text{S23})$$

where

$$F(t) = \frac{1}{\mathcal{Z}(t)} \frac{d}{dt} e^{A(t)} = \int_0^1 \rho(t)^s E \rho(t)^{1-s} ds. \quad (\text{S24})$$

By Lemma S2,  $\|F(t)\|_1 \leq \|E\|_\infty$ . In addition,

$$\mathrm{Tr}[F(t)] = \int_0^1 \mathrm{Tr}[\rho(t)^s E \rho(t)^{1-s}] \, ds = \int_0^1 \mathrm{Tr}[\rho(t)E] \, ds = \mathrm{Tr}[\rho(t)E] \leq \|E\|_\infty. \quad (\text{S25})$$

Therefore  $\|\frac{d}{dt}\rho(t)\|_1 \leq 2\|E\|_\infty$  for all  $t \in [0, 1]$ , and integrating over  $t$  yields

$$\|\rho(1) - \rho(0)\|_1 \leq 2\|E\|_\infty, \quad (\text{S26})$$

as claimed.  $\blacksquare$

The main error bound is stated and proved below. The argument is most informative when indices repeat frequently (i.e.,  $N \gg \max(L, n)$ ), where the palindromic product can be compared sharply with an exponential via higher-order BCH control, yielding a tighter bound than a second-order Trotter decomposition [39].

**Theorem 1 (Complete version of Theorem 1)** *Let  $N = \Omega(n\lambda^2\beta^2)$  and  $\delta > 0$ . Then  $\rho_N$  in Equation (S3) and  $G_{\beta, H}$  in Equation (S6) satisfy*

$$\mathrm{Pr}\left(\|\rho_N - G_{\beta, H}\|_1 > \mathcal{O}\left(K_0^{3/2} N^{3/2} \tau^3\right)\right) \leq \delta \quad (\text{S27})$$

for  $K_0 = (n+2)\log 2 + \log(N/\delta)$ .

**Proof** Denote  $S_k = \sum_{i=1}^k B_i$ . By Lemma S10,

$$E := 2S_N - \log \left( \left( \prod_{k=N}^2 e^{B_k} \right) e^{2B_1} \left( \prod_{k=2}^N e^{B_k} \right) \right) = \frac{1}{3} (E_1 - 2E_2) - R_N \quad (\text{S28})$$

for  $E_1 = \sum_{k=2}^N [B_k, [B_k, S_{k-1}]]$ ,  $E_2 = \sum_{k=2}^N [S_{k-1}, [B_k, S_{k-1}]]$  and some remainder term  $R_N$ . Lemma S11 reduces the trace-norm comparison to a spectral-norm bound on  $E$ :

$$\|\rho_N - G_{\beta, H}\|_1 = \left\| \frac{e^{\log \left( \prod_{k=N}^2 e^{B_k} \right) e^{2B_1} \left( \prod_{k=2}^N e^{B_k} \right)}}{\mathrm{Tr}[\text{same above}]} - \frac{e^{E + \log \left( \prod_{k=N}^2 e^{B_k} \right) e^{2B_1} \left( \prod_{k=2}^N e^{B_k} \right)}}{\mathrm{Tr}[\text{same above}]} \right\|_1 \leq 2\|E\|_\infty. \quad (\text{S29})$$

It therefore suffices to upper bound  $\|E_1\|_\infty$ ,  $\|E_2\|_\infty$ , and  $\|R_N\|_\infty$  with high probability, and then combine these bounds.

We begin by controlling  $\|S_k\|_\infty$ . Let  $\mathcal{F}_k = (B_i)_{i=1}^k$  be the natural filtration, define the drift  $D_k = \mathbb{E}[B_k | \mathcal{F}_{k-1}]$ , and let  $M_k = B_k - D_k$ . Then  $S_k = \sum_{i=1}^k D_i + \sum_{i=1}^k M_i$ . For the drift term, we have

$$\|D_k\|_\infty = \|\mathbb{E}[B_k | \mathcal{F}_{k-1}]\|_\infty = \left\| \left[ \frac{\mathrm{Tr}[e^{\tau\sigma_{j_k}} \rho_{k-1}]}{2 \cosh \tau} - \frac{\mathrm{Tr}[e^{-\tau\sigma_{j_k}} \rho_{k-1}]}{2 \cosh \tau} \right] \cdot \frac{\tau\sigma_{j_k}}{2} \right\|_\infty \quad (\text{S30})$$

$$\leq |\mathrm{Tr}[e^{\tau\sigma_{j_k}} \rho_{k-1}] - \mathrm{Tr}[e^{-\tau\sigma_{j_k}} \rho_{k-1}]| \cdot \frac{\tau}{4 \cosh \tau} \quad (\text{S31})$$

$$= |(e^\tau - e^{-\tau}) \mathrm{Tr}[\sigma_{j_k} \rho_{k-1}]| \cdot \frac{\tau}{2(e^\tau + e^{-\tau})} \quad (\text{S32})$$

$$\leq \frac{1}{2}\tau \tanh \tau = \tau^2 + \mathcal{O}(\tau^4) < 0.1\tau, \quad (\text{S33})$$

for  $\tau \ll 1$ . The sequence  $(M_k)_k$  is a martingale difference sequence of Hermitian matrices with respect to  $(\mathcal{F}_k)_k$ , since  $\mathbb{E}[M_k | \mathcal{F}_{k-1}] = 0$ . In particular,  $\|M_k\|_\infty \leq \|B_k\|_\infty + \|D_k\|_\infty \leq \tau + 0.1\tau = 1.1\tau$ . Applying Lemma S4, for any  $k$  and  $t_k > 0$ ,

$$\mathrm{Pr}\left(\left\| \sum_{i=1}^k M_i \right\|_\infty > t_k \text{ and } \left\| \sum_{i=1}^k \mathbb{E}[M_i^2 | \mathcal{F}_{i-1}] \right\|_\infty \leq \frac{k\tau^2}{4}\right) \leq 2^{n+1} \exp\left(-\frac{t_k^2/2}{k\tau^2/4 + 1.1\tau t_k/3}\right). \quad (\text{S34})$$

We also have

$$\sum_{i=1}^k \mathbb{E}[M_i^2 | \mathcal{F}_{i-1}] = \sum_{i=1}^k \mathbb{E}[B_i^2 | \mathcal{F}_{i-1}] - D_i^2 = \sum_{i=1}^k \frac{\tau^2}{4} I - D_i^2 \quad (\text{S35})$$

$$\implies \left\| \sum_{i=1}^k \mathbb{E}[M_i^2 | \mathcal{F}_{i-1}] \right\|_\infty \leq \sum_{i=1}^k \left\| \frac{\tau^2}{4} I - D_i^2 \right\|_\infty \leq \sum_{i=1}^k \left\| \frac{\tau^2}{4} I \right\|_\infty = \frac{k}{4} \tau^2, \quad (\text{S36})$$

so choosing  $K = (n+1) \log 2 + \log \delta^{-1}$  and  $t_k = \tau \sqrt{kK/2} + 2.2\tau K/3$  implies  $(t_k/\tau)^2/(k/2 + \frac{2.2}{3}t_k/\tau) \geq K$ , and therefore

$$\Pr\left(\left\| \sum_{i=1}^k M_i \right\|_\infty > t_k\right) \leq 2^{n+1} \exp\left(-\frac{t_k^2}{k\tau^2/2 + 2.2\tau t_k/3}\right) = 2^{n+1} \exp\left(-\frac{(t_k/\tau)^2}{k/2 + 2.2/3 \cdot (t_k/\tau)}\right) \quad (\text{S37})$$

$$\leq 2^{n+1} e^{-K} = \delta. \quad (\text{S38})$$

Combining the drift and martingale parts yields

$$\|S_k\|_\infty \leq \left\| \sum_{i=1}^k M_i \right\|_\infty + \sum_{i=1}^k \|D_i\|_\infty \implies \Pr(\|S_k\|_\infty > t_k + k\tau^2) \leq \delta. \quad (\text{S39})$$

We next bound  $\|E_1\|_\infty$ . Since  $B_k \sim \{\tau\sigma_{j_k}/2, -\tau\sigma_{j_k}/2\}$ ,

$$\|E_1\|_\infty = \left\| \sum_{k=2}^N [B_k, [B_k, S_{k-1}]] \right\|_\infty \quad (\text{S40})$$

$$\leq \sum_{k=2}^N \|[B_k, [B_k, S_{k-1}]]\|_\infty = \sum_{k=2}^N \|B_k^2 S_{k-1} + S_{k-1} B_k^2 - 2B_k S_{k-1} B_k\|_\infty \quad (\text{S41})$$

$$= \frac{\tau^2}{2} \sum_{k=2}^N \|S_{k-1} - \sigma_{j_k} S_{k-1} \sigma_{j_k}\|_\infty \leq \tau^2 \sum_{k=2}^N \|S_{k-1}\|_\infty \quad (\text{S42})$$

$$\implies \Pr\left(\|E_1\|_\infty > \tau^2 \sum_{k=2}^N (t_k + k\tau^2)\right) \leq \delta. \quad (\text{S43})$$

The term  $E_2$  is handled in a similar way. Assume  $\|S_k\|_\infty \leq t_k + k\tau^2$  (we account for this event in the final probability bound). Define  $Q_k = [S_k, [M_{k+1}, S_k]]$ , so that

$$[S_{k-1}, [B_k, S_{k-1}]] = Q_{k-1} + [S_{k-1}, [D_k, S_{k-1}]] \quad (\text{S44})$$

with  $\|[S_{k-1}, [D_k, S_{k-1}]]\|_\infty \leq 4\|S_k\|_\infty^2 \|D_{k+1}\|_\infty = 4(t_k + k\tau^2)^2 \tau^2$ . One can verify that  $\mathbb{E}[Q_k | \mathcal{F}_k] = 0$  and

$$\|Q_k\|_\infty \leq 4\|S_k\|_\infty^2 \|M_{k+1}\|_\infty = 4.4(t_k + k\tau^2)^2 \tau, \quad (\text{S45})$$

$$\|\mathbb{E}[Q_k^2 | \mathcal{F}_{k-1}]\|_\infty \leq 4\|S_k\|_\infty^4 \|M_{k+1}\|_\infty^2 \leq 20(t_k + k\tau^2)^4 \tau^2, \quad (\text{S46})$$

$$\left\| \sum_{k=1}^N \mathbb{E}[Q_k^2 | \mathcal{F}_{k-1}] \right\|_\infty \leq 20N(t_N + N\tau^2)^4 \tau^2. \quad (\text{S47})$$

Lemma S4 therefore implies that, for any  $k$  and  $s_k > 0$ ,

$$\Pr\left(\left\| \sum_{i=1}^k Q_i \right\|_\infty > s_k\right) \leq 2^{n+1} \exp\left(-\frac{s_k^2/2}{20N(t_N + N\tau^2)^4 \tau^2 + 4.4(t_k + k\tau^2)^2 \tau s_k/3}\right). \quad (\text{S48})$$

Taking  $s_k = \sqrt{40KN}(t_N + N\tau^2)^2 \tau + 8.8(t_k + k\tau^2)^2 K \tau / 3$  simplifies the bound to

$$\Pr\left(\left\| \sum_{i=1}^k Q_i \right\|_\infty > s_k\right) \leq 2^{n+1} e^{-K} \leq \delta. \quad (\text{S49})$$

Consequently,

$$\|E_2\|_\infty = \left\| \sum_{k=2}^N [S_{k-1}, [B_k, S_{k-1}]] \right\|_\infty \leq \left\| \sum_{k=2}^N Q_{k-1} \right\|_\infty + \sum_{k=2}^N \|[S_{k-1}, [D_k, S_{k-1}]]\|_\infty \quad (\text{S50})$$

$$\implies \Pr\left(\|E_2\|_\infty > s_N + 4 \sum_{k=2}^N (t_k + k\tau^2)^2 \tau^2\right) \leq \delta. \quad (\text{S51})$$

We now combine the bounds. Since  $N \gg n$ , for all  $k \leq N$  we have  $t_k + k\tau^2 \leq t_N + N\tau^2 = \mathcal{O}(\tau\sqrt{NK}) + N\tau^2 = \mathcal{O}(\tau\sqrt{NK})$ . Therefore,  $\|E_1\|_\infty \leq \tau^2 \sum_{k=2}^N (t_k + k\tau^2) = \mathcal{O}(N\tau^3\sqrt{NK})$  and  $\|E_2\|_\infty \leq s_N + 4 \sum_{k=2}^N (t_k + k\tau^2)^2 \tau^2 = \mathcal{O}(\tau^3 K^{3/2} N^{3/2})$ , which implies  $\|E_1 - 2E_2\|_\infty = \mathcal{O}(\tau^3 K^{3/2} N^{3/2})$ .

It remains to bound the remainder term. By Lemma S10,

$$\|\mathcal{R}_N\|_\infty = \mathcal{O}\left(\sum_{r=5, r \text{ is odd}}^{\infty} \frac{1}{r!} \sum_{k=2}^N \|\text{ad}_{2S_{k-1}}^{r-1}(B_k)\|_\infty\right). \quad (\text{S52})$$

For an odd order  $r \geq 5$ , applying Lemma S4 yields

$$\frac{1}{r!} \sum_{k=2}^N \|\text{ad}_{2S_{k-1}}^{r-1}(B_k)\|_\infty = \frac{2^r}{r!} \mathcal{O}((\sqrt{NK}\tau)^r) = o(\tau^3 K^{3/2} N^{3/2}). \quad (\text{S53})$$

Alternatively, the triangle inequality gives

$$\frac{1}{r!} \sum_{k=2}^N \|\text{ad}_{2S_{k-1}}^{r-1}(B_k)\|_\infty = \frac{2^{2r}}{r!} \mathcal{O}(N\tau(\sqrt{NK}\tau)^{r-1}). \quad (\text{S54})$$

For  $r^* = \left\lceil \frac{\log(K\tau^2\sqrt{NK})}{\log(\tau\sqrt{NK})} \right\rceil$ , this implies  $\|\mathcal{R}_N\|_\infty = \mathcal{O}(\tau^3 K^{3/2} N^{3/2})$ . We therefore apply Lemma S4 for  $r < r^*$  and use the triangle inequality for  $r \geq r^*$ ; the remaining tail ( $r > r^*$ ) decays exponentially and can be neglected at the stated precision.

Substituting these bounds into  $\|\rho_N - G_{\beta, H}\|_1 \leq 2\|E\|_\infty$  yields

$$\Pr\left(\|\rho_N - G_{\beta, H}\|_1 \leq \mathcal{O}(K^{3/2} N^{3/2} \tau^3)\right) \geq 1 - \delta. \quad (\text{S55})$$

It remains to account for the overall failure probability. The proof applies Lemma S4  $(r^* - 1)/2 + N$  times. Setting  $\delta' = \delta/((r^* - 1)/2 + N)$  and taking a union bound ensures that the total failure probability is at most  $\delta$ . Under this rescaling,  $K = (n + 1) \log 2 + \log(((r^* - 1)/2 + N)/\delta)$ . Given  $N \gg n$  and  $\tau\sqrt{NK} \ll 1$ , we may assume  $N \gg K$  and obtain

$$r^* \leq 2 + \frac{\log(K\tau)}{\log(\tau\sqrt{NK})} \ll N, \quad (\text{S56})$$

which implies  $K \leq (n + 2) \log 2 + \log(N/\delta) \ll N$ . Taking  $K_0 = (n + 2) \log 2 + \log(N/\delta)$  therefore yields the stated bound.  $\blacksquare$

## 2. Sample distribution

Recall that Algorithm 1 generates a path  $\mathcal{P} = ((j_1, m_1), \dots, (j_N, m_N)) \in [L] \times \{1, -1\}$ . In Section C1, we assumed  $\mathcal{P}$  is fixed so that the evolution sequence can be analyzed without randomness. This section uses a random walk to incorporate the randomness of  $j_k$  and  $m_k$ .

Consider how the sampled Hamiltonian evolves as the path develops. Stopping the algorithm at step  $k \in [N]$  yields the intermediate Hamiltonian  $H^{(k)} = \sum_{t=1}^k m_t \sigma_{j_t}$ . The sampling process can thus be described as a sequence  $(H^{(k)})_k$ , with  $H^{(N)}$  being the final output. Equivalently, this sequence is a random walk on a lattice:

$$\mathbf{x}^{(k)} = \sum_{t=1}^k m_t e_{j_t} \in \{-N, \dots, N\}^{\times L}, \quad \mathbf{x}^{(0)} = 0, \quad (\text{S57})$$

where  $e_{j_t}$  is the standard vector in the lattice corresponding to  $\sigma_{j_t}$ , and every forward step satisfies

$$\Pr\left(\mathbf{x}^{(k)} - \mathbf{x}^{(k-1)} = \pm e_j\right) = \Pr(m_k = \pm 1) \cdot h_j/\lambda. \quad (\text{S58})$$

The sign of  $m_k$  is determined by the quantum measurement in Theorem S7, which is difficult to analyze directly. We therefore introduce a reference probability measure  $Q$  with  $\Pr_Q(m_k = \pm 1) = 1/2$ , giving

$$\Pr_Q\left(\mathbf{x}^{(k)} - \mathbf{x}^{(k-1)} = \pm e_j\right) = h_j/2\lambda \quad (\text{S59})$$

corresponding to  $N \rightarrow \infty$ . The relation between the reference probability measure and the true probability measure is stated by the likelihood ratio  $L_N(\mathcal{P}) = \Pr(\mathcal{P}) / \Pr_Q(\mathcal{P})$  in the following statement.

**Lemma S13** *If  $N = \Omega(n\lambda^2\beta^2)$ , then for  $H = H^{(N)}$ ,*

$$\log L_N(\mathcal{P}) = \log\left(\frac{1}{2^n} \text{Tr}[e^{-\beta H}]\right) + \mathcal{O}\left(\frac{\lambda^2\beta^2}{N}\right). \quad (\text{S60})$$

**Proof** For convenience, denote  $\rho_{\mathbf{x}}$  as the thermal state of Hamiltonian with respect to  $\mathbf{x}$  and  $M_j(\mathbf{x}) = \text{Tr}[\sigma_j \rho_{\mathbf{x}}]$ . By Theorem S7, the outcome distribution at step  $t$  given the Pauli operator  $\sigma_{j_t}$  can be written as

$$\Pr(m_t = \pm 1 \mid j_t) = \frac{1}{2} \left( 1 \mp \tanh \tau \text{Tr} \left[ \sigma_{j_t} M_j(\mathbf{x}^{(t-1)}) \right] \right) \quad (\text{S61})$$

Since  $\Pr_Q(m_t = \pm 1 \mid j_t) = 1/2$  and the probabilities for sampling  $j_t$  for both measures are the same, the likelihood ratio takes the product form

$$L_N(\mathcal{P}) = 2^N \prod_{t=1}^N \Pr(m_t = \pm 1 \mid j_t) = \prod_{t=1}^N \left( 1 - m_t \tanh(\tau) M_{j_t}(\mathbf{x}^{(t-1)}) \right). \quad (\text{S62})$$

Using  $\log(1 + y) = y + \mathcal{O}(y^2)$  and  $\tanh \tau = \tau + \mathcal{O}(\tau^3)$  gives

$$\log L_N(j, m) = -\tau \sum_{t=1}^N m_t M_{j_t}(\mathbf{x}^{(t-1)}) + \mathcal{O}(N\tau^2). \quad (\text{S63})$$

Denote the partition function of  $H^{(t)}$  at the  $t$ -th step as

$$\mathcal{Z}(\mathbf{x}^{(t)}) = \text{Tr} \left[ \exp \left( -\beta H^{(t)} \right) \right] = \text{Tr} \left[ \exp \left( -\tau \sum_{j=1}^L \mathbf{x}_j^{(t)} \sigma_j \right) \right]. \quad (\text{S64})$$

Observe that differentiating  $\log \mathcal{Z}(\mathbf{x})$  with respect to  $\mathbf{x}_j$  gives

$$\partial_{\mathbf{x}_j} \log \mathcal{Z}(\mathbf{x}) = \frac{1}{\mathcal{Z}(\mathbf{x})} \text{Tr} \left[ (-\tau \sigma_j) \exp \left( -\tau \sum_{j=1}^L \mathbf{x}_j \sigma_j \right) \right] = -\tau M_j(\mathbf{x}). \quad (\text{S65})$$

Therefore, since  $\mathbf{x}^{(t)} - \mathbf{x}^{(t-1)} = m_t e_{j_t}$ ,

$$-\tau m_t M_{j_t}(\mathbf{x}^{(t-1)}) = m_t \partial_{\mathbf{x}^{(t-1)}} \log \mathcal{Z}(\mathbf{x}^{(t-1)}) = \nabla_{\mathbf{x}} \log \mathcal{Z}(\mathbf{x}^{(t-1)}) \cdot (\mathbf{x}^{(t)} - \mathbf{x}^{(t-1)}). \quad (\text{S66})$$

Because  $\mathcal{Z}(\mathbf{x})$  depends on  $\mathbf{x}$  through  $\tau \mathbf{x}$  and  $\tau \ll 1$ , a Taylor expansion of  $\log \mathcal{Z}$  along one lattice step gives

$$\log \mathcal{Z}(\mathbf{x}^{(t)}) - \log \mathcal{Z}(\mathbf{x}^{(t-1)}) = \nabla_{\mathbf{x}} \log \mathcal{Z}(\mathbf{x}^{(t-1)}) \cdot (\mathbf{x}^{(t)} - \mathbf{x}^{(t-1)}) + \mathcal{O}(\tau^2). \quad (\text{S67})$$

Summing over  $t = 1, \dots, N$  and substituting into Equation (S63) yields

$$\log L_N(j, m) = \log \mathcal{Z}(\mathbf{x}^{(N)}) - \log \mathcal{Z}(0) + \mathcal{O}(N\tau^2). \quad (\text{S68})$$

Finally,  $\mathcal{Z}(0) = \text{Tr}[I] = 2^n$  and  $\mathcal{Z}(\mathbf{x}^{(N)}) = \text{Tr} \left[ \exp(-\tau \sum_j \mathbf{x}_j \sigma_j) \right] = \text{Tr} \left[ e^{-\beta H^{(N)}} \right]$ , so the statement follows from  $N\tau^2 = \lambda^2\beta^2/N$ .  $\blacksquare$

We now state the theoretical result for the sample distribution.

**Theorem 2 (Complete version of Theorem 2)** Suppose  $n \gg 1$  and  $N = \Omega(n\lambda^2\beta^2)$ . Let  $H = \sum_{j=1}^L c_j \sigma_j$  and  $p_j = c_j/\lambda$ . When  $\sum_j c_j^2 \leq N\lambda^2$ , the datum  $(H, G_{\beta, H})$  can be sampled by Algorithm 1 with probability proportional to  $\frac{1}{2^n} \text{Tr}[e^{-\beta H}] \cdot D(\mathbf{x})$ , where  $D$  is given as

$$D(\mathbf{x}) = \frac{a_N(\mathbf{x})}{(2\pi N)^{L/2} \sqrt{\prod_{j=1}^L p_j}} \exp\left(-\frac{1}{2N} \sum_j p_j \mathbf{x}_j^2\right) + o(N^{-L/2}). \quad (\text{S69})$$

**Proof** Fix  $H = \sum_{j=1}^L c_j \sigma_j$  on the output grid, and let  $\mathbf{x} \in \mathbb{Z}^L$  be the corresponding endpoint vector  $\mathbf{x}_j = c_j N/\lambda$ . Denote  $\mathcal{P}_{\mathbf{x}}$  the set of paths whose endpoint equals  $\mathbf{x}$ . Then the event that Algorithm 1 returns  $H$  is exactly the endpoint event  $\mathbf{x}^{(N)} = \mathbf{x}$ .

By definition of the likelihood ratio and Lemma S13,

$$\Pr(\mathcal{P}) = \Pr_Q(\mathcal{P}) \cdot \exp\left(\log\left(\frac{1}{2^n} \text{Tr}[e^{-\beta H}]\right) + \mathcal{O}\left(\frac{\lambda^2\beta^2}{N}\right)\right). \quad (\text{S70})$$

When  $\|\mathbf{x}\| = \mathcal{O}(\sqrt{N})$ . Therefore, absorbing the  $\mathbf{x}$ -independent normalization into the proportionality constant, summing over all  $\mathcal{P}$  with same endpoint, we obtain

$$\begin{aligned} \Pr(\mathbf{x}^{(N)} = \mathbf{x}) &= \exp\left(\log\left(\frac{1}{2^n} \text{Tr}[e^{-\beta H}]\right) + \mathcal{O}\left(\frac{\lambda^2\beta^2}{N}\right)\right) \cdot \sum_{\mathcal{P} \in \mathcal{P}_{\mathbf{x}}} \Pr_Q(\mathcal{P}) \\ &\propto \frac{1}{2^n} \text{Tr}[e^{-\beta H}] \cdot \Pr_Q(\mathbf{x}^{(N)} = \mathbf{x}). \end{aligned} \quad (\text{S71})$$

Denote  $D(\mathbf{x}) = \Pr_Q(\mathbf{x}^{(N)} = \mathbf{x})$ . Substituting Lemma S5 yields the Gaussian approximation claimed in the theorem.  $\blacksquare$

#### Appendix D: Experimental setting

This section provides the numerical settings used in each experiment. All experiments are performed on a  $3 \times 3$  two-dimensional grid of  $n = 9$  qubits, with sites labeled  $1, \dots, 9$  in row-major order. The nearest-neighbor pairs  $\langle i, j \rangle$  consist of 12 edges connecting horizontally and vertically adjacent sites. For the Heisenberg ensemble, the sampled Hamiltonians take the form

$$H_{\text{Heis}} = \sum_{\langle i, j \rangle} \left( c_{ij}^{(X)} X_i X_j + c_{ij}^{(Y)} Y_i Y_j + c_{ij}^{(Z)} Z_i Z_j \right), \quad (\text{S1})$$

where the coefficients  $c_{ij}^{(\alpha)}$  are generated by the sampling algorithm and satisfy  $|c_{ij}^{(\alpha)}| \leq h$  for a uniform bound  $h > 0$ . For the transverse-field Ising ensemble, the sampled Hamiltonians take the form

$$H_{\text{Ising}} = \sum_{\langle i, j \rangle} c_{ij} Z_i Z_j + \sum_{i=1}^n g_i X_i, \quad (\text{S2})$$

where the coefficients  $c_{ij}$  and  $g_i$  are similarly bounded. In both cases,  $\lambda = \sum_j h_j$  denotes the sum of all coefficient bounds. Throughout, we set the step-number constant  $C = \lambda^2/\epsilon_0^{2/3}$  with target precision  $\epsilon_0 = 10^{-6}$ .

For Figure 2, all three panels use the Heisenberg ensemble with the maximally mixed state  $I/d$  as the initial state. In panel (a), we scan the inverse temperature from  $\beta = 1$  to  $\beta = 10$  and test three scaling exponents  $k \in \{1.5, 2.0, 2.5\}$ , which define the step number as  $N = C\beta^k$ . For each parameter pair  $(\beta, N)$ , we perform 100 independent sampling runs and record the maximal trace-distance error  $\epsilon$  among the samples. Panels (b) and (c) both fix  $\beta = 2$ . In panel (b), we set  $N = C\beta^2$  and generate 10 000 independent samples to obtain the empirical coefficient distribution; the theoretical curve is computed from the normal distribution predicted by Theorem 2, reweighted by the thermal partition function and estimated via Monte Carlo with 10 000 samples. In panel (c), we scan the scaling exponent  $k$  from 1 to 3 and perform 100 independent runs for each  $N = C\beta^k$ . The inverse precision is defined as  $1/\epsilon$ , where  $\epsilon$  is the maximal trace-distance error among the samples. The effective sample range is quantified by the operator norm  $\|H\|_{\infty}$  of each sampled Hamiltonian; we report the sample mean and standard error over the ensemble.

For Figure 3, we use the transverse-field Ising ensemble to generate the output states. The initial state is a thermal state of a Heisenberg Hamiltonian, whose modular spectrum exhibits near-Poisson statistics in this finite-size setting. We fix  $\beta = 2$  and  $N = C\beta^2$ , and perform 20 independent sampling runs. For each output state  $\rho$ , we define the modular Hamiltonian  $K = -\log \rho$  and compute the adjacent gap-ratio statistic  $r$  from the spectrum of  $K$ . To handle near-degeneracies, eigenvalues within a relative tolerance of  $10^{-6}$  are merged into a single representative level before evaluating the spacing ratios. The resulting  $r$  values are aggregated over all samples to form the final histogram.